THEORETICAL STUDY OF HETEROGENEOUS FACTORS IN EPIDEMIOLOGICAL MODELS

大森, 亮介
九州大学大学院システム生命科学府

https://doi.org/10.15017/21711

出版情報：九州大学, 2011, 博士（理学）, 課程博士
バージョン：
権利関係：

Theoretical study of heterogeneous factors in epidemiological models

Ryosuke Omori

Submitter to the faculty of Graduate School of Kyushu University

In partial fulfillment of the requirements

For degree of

Doctor of Science in Biology

Systems Life Sciences, Kyushu University

December, 2011

Contents

Acknowledgements

Preface

In epidemiology, or the study of public health in a population, theoretical approaches have been quite useful in the prevention or suppression of infectious diseases. Theoretical epidemiology consists of constructing mathematical and computational models, estimating parameters from statistical data, forecasting the spread of diseases, and examining the effectiveness of alternative policies. This gives estimates of key quantities such as basic reproductive number, final epidemic size and epidemic duration. Dynamics of susceptible, infected and recovered host, often called SIR model, and the diffusion process model describing the spread and the extinction of infectious diseases are the two classical models but still play important roles in theoretical epidemiology.

Using the simplest SIR model, epidemic peak timing, prevalence at epidemic peak timing, final epidemic size and frequency of vaccinated host for prevention of outbreak can be solved analytically (Anderson and May 1991). However, this model is often difficult to apply directly to real epidemics, because of various factors causing heterogeneity. The basic SIR model includes many approximations and neglects heterogeneous factors. These simplifications sometimes are unrealistic when it is applied to real epidemics. For example, the basic model assumes that transmission rate is constant over time, but most epidemics show clear seasonality, demonstrating annual outbreaks. To cope with this situation, some theoretical studies analyzed the dynamics of reemergence of epidemics by assuming that the transmission rate is a simple periodic function of time. This makes the analysis of dynamics difficult mathematically, even if a periodic function of transmission rate is a sinusoidal function of time. Furthermore the results in this model are sometimes quite different from basic model, demonstrating for example periodic outbreaks with period longer then one year or chaotic fluctuations.

Second, the transmission rate as a function of time may differ between strains of pathogens and also strains of hosts. As a result of invasion of new strains and replacement, the transmission rate should change over time, and this is a coevolutionary processes, as both pathogens and hosts evolve simultaneously. Human and other vertebrate have acquired immunity, which allow a much quicker adaptation to the change in the pathogen fauna, and the study of host-pathogen coevolution must consider acquired immunity of the host.

Third, perfect specificity is often assumed in the basic SIR model but cross reaction should play very important role in multi-strain systems. Cross reactive immune reaction usually protects hosts from infection with other strains that are similar to the original type, but sometimes enhances infection with other very different strains, called antibody-dependent enhancement. This aspect of immunity complicates the dynamics of epidemics because the transmission rate of each strain is determined by complicated genetic relationship between current strain and past strains that host had infected (chapter 1 and 2). Heterogeneity in host contact network changes not only final epidemic size and epidemic duration but also the fate of evolution of pathogen.

Fourth, the simplest SIR model assumes complete graph in host contact network, but real host contact network is not homogeneous and changes over time. Details of the population dynamics of pathogen within hosts are emerging in recent studies and we can construct more precise mathematical models, and the results in these models are sometimes quite different from results in classical models (chapter 3). Age of host is not assumed in basic model, however, it is important for analysis of reemergence of epidemics when acquired immunity wanes. We need to understand effects of these heterogeneous factors in epidemiological models to dynamics of epidemics and extend classical model with that for application to real epidemics.

The objective of this thesis is to illustrate how different heterogeneous factors affect the dynamics and evolution of infectious diseases. I especially focus on the following three aspects: i) co-evolution between host immunity and pathogen, ii) seasonality of epidemics, and iii) population dynamics of pathogen within hosts. I summarize the contents for chapters as follows:

Chapter 1: Coexistence condition for strains with immune cross-reaction

The accumulation of cross-immunity in the host population is an important factor driving the antigenic evolution of viruses such as influenza A. Mathematical models have shown that the strength of temporary non-specific cross-immunity and the basic reproductive number are both key determinants for evolutionary branching of the antigenic phenotype. Here we develop deterministic and stochastic versions of one such model. We examine how the time of emergence or introduction of a novel strain affects co-existence with existing strains and hence the initial establishment of a new evolutionary branch. We also clarify the roles of cross-immunity and the basic

reproductive number in this process. We show that the basic reproductive number is important because it affects the frequency of infection, which influences the long term immune profile of the host population. The time at which a new strain appears relative to the epidemic peak of an existing strain is important because it determines the environment the emergent mutant experiences in terms of the short term immune profile of the host population. Strains are more likely to coexist, and hence to establish a new clade in the viral phylogeny, when there is a significant time overlap between their epidemics. It follows that the majority of antigenic drift in influenza is expected to occur in the earlier part of each transmission season and this is likely to be a key surveillance period for detecting emerging antigenic novelty.

Chapter 2: The timing of the emergence of new successful strains in seasonal influenza

High evolvability of influenza virus and the complex nature of its antagonistic interaction with host immune system make it difficult to predict what strain of virus will become epidemic next and when it will emerge. To investigate the most likely timing at which a new successful strain emerges ever year in seasonal influenza, we here study an individual base model that takes into account the seasonality in transmission rate and the cross-immunity of host individual against a current viral strain due to the past infections of other strains. The model we consider in the paper deals with antigenic evolution of influenza that is originated by point mutations at epitope sites and driven by host immune response. Under the range of parameters at which influenza viral population shows a “trunk” shape in the phylogenetic tree, as is typical in influenza A virus evolution, we found that most successful mutant strains emerge in an early period of the epidemic season, and that the timing when the number of the hosts infected by them reach the maximum tends to be more than one season after the emergence. This carry over of the epidemic peak timing implies that we can detect the strain that will become dominant epidemic in the next year.

Chapter 3: Disrupting seasonality to control disease outbreaks: the case of koi herpes virus

Common carp accounts for a substantial proportion of global freshwater aquaculture production. Koi herpes virus (KHV), a highly virulent disease affecting

carp that emerged in the late 1990s, is a serious threat to this industry. After a fish is infected with KHV, there is a temperature dependent delay before it becomes infectious, and a further delay before mortality. Consequently, KHV epidemiology is driven by seasonal changes in water temperature. Also, it has been proposed that outbreaks could be controlled by responsive management of water temperature in aquaculture setups. We use a mathematical model to analyse the effect of seasonal temperature cycles on KHV epidemiology, and the impact of attempting to control outbreaks by disrupting this cycle. We show that, although disease progression is fast in summer and slow in winter, total mortality over a 2-year period is similar for outbreaks that start in either season. However, for outbreaks that start in late autumn, mortality may be low and immunity high. A single bout of water temperature management can be an effective outbreak control strategy if it is started as soon as dead fish are detected and maintained for a long time. It can also be effective if the frequency of infectious fish is used as an indicator for the beginning of treatment. In this case, however, there is a risk that starting the treatment too soon will increase mortality relative to the case when no treatment is used. This counterproductive effect can be avoided if multiple bouts of temperature management are used. We conclude that disrupting normal seasonal patterns in water temperature can be an effective strategy for controlling koi herpes virus. Exploiting the seasonal patterns, possibly in combination with temperature management, can also induce widespread immunity to KHV in a cohort of fish. However, employing these methods successfully requires careful assessment to ensure that the treatment is started, and finished, at the correct time.

Chapter 1

Coexistence conditions for strains of influenza with immune cross-reaction

The study of this chapter, done in collaboration with Dr. Ben Adams and Prof. Akira Sasaki, was published in Journal of Theoretical Biology (262, pp48-57) in 2010.

Introduction

One of the most striking characteristics of the influenza A virus is its extraordinarily rapid evolution due to strong selection mediated by the host immune response to viral antigens. If a strain of influenza causes a large epidemic, the majority of hosts acquire immunity against that strain. In order to be successful, subsequent viral strains must therefore escape the residual host immunity and this promotes the fixation of mutants with novel epitopes. A key feature of influenza A evolution is that, despite the appearance and spread of new strains each year, the vast majority become rapidly extinct and the number of persistent branches in the phylogenetic tree remains small (Bush et al. 1999; Smith et al. 2004; Holmes et al. 2005). One of the most important factors responsible for maintaining this slim phylogenetic tree is likely to be cross-immunity (Andreasen et al. 1997; Ferguson et al. 2003; Koelle et al. 2006; Andreasen and Sasaki. 2006), whereby infection with one strain suppresses subsequent infections with antigenically similar strains. Cross-immunity is a major determinant of phylogenetic branching because it can make it difficult for a mutant strain to coexist with the parental or sibling strains.

A key feature of influenza dynamics is the strong seasonality of incidence in temperate regions. To understand the ecology and evolution of influenza, it is vital to understand the way in which host immunity mediates the epidemiological and antigenic interaction of viral strains in the context of seasonal epidemics. An earlier study (Andreasen and Sasaki. 2006) considered a simple model in which discrete annual epidemics of influenza were assumed to be caused by antigenic variants derived from a common ancestor in the previous year. The variants occupied a low-dimensional antigenic space and emerged serially to cause sequential, non-overlapping epidemics. This analysis indicated that strong temporary broad cross-immunity between all viral strains, a high basic reproductive rate and rapid decay in long term strain specific cross-immunity are required to prevent evolutionary branching and maintain the slim antigenic phylogeny of influenza (Andreasen and Sasaki. 2006). Empirical studies, however, show that antigenic variants do not appear in strict sequence each season and there may be extensive co-circulation. In New York State two distinct clades of H3N2 co-circulated in the 2002 – 2003 transmission season and three distinct clades circulated in the 2003 – 2004 season (Holmes et al. 2005). In the 2006 – 2007 season multiple co-circulating clades causing overlapping epidemics were detected (Nelson et al. 2008).

In each season each clade is believed to have arisen from a novel introduction (Nelson et al. 2006; 2008).

There are many complex factors governing the epidemiology and evolution of influenza. Here we will focus on the roles that seasonal epidemics and the extent of co-circulation pf antigenic variants play in antigenic branching. We show that partially over-lapping epidemics can enhance co-existence of antigenic variants, making branching more likely. This effect is strongly dependent on the time lag between the introduction of each variant. It may also be moderated by season to season variation in the sequence in which variants appear. Nevertheless maintenance of the characteristic unbranched phylogeny of influenza may require a higher basic reproductive number or stronger broad cross-immunity than anticipated by previous work.

Models based on linear antigenic spaces are often used to analyze the coupled dynamics of the host population immune profile and the antigenic properties of the influenza virus (Sasaki. 1994; Andreasen et al. 1996; Haraguchi and Sasaki. 1997; Gog and Grenfell. 2002; Andreasen. 2003; Lin et al. 2003; Boni et al. 2004; Adams and Sasaki. 2007;) because the antigenic drift of influenza A shows approximately linear evolution along a single phylogenetic trunk. However, antigen characteristics are thought to be high dimensional (Smith et al. 2004) and other approaches define antigenic types based on abstractions of the epitope sequence (Sasaki and Haraguchi. 2000; Ferguson et al. 2003; Tria et al. 2005; Adams and Sasaki. 2009). Therefore, we also use an individual-based simulation of the epidemic model to consider the effect of modeling the antigenic evolution through a high dimensional antigenic space. We find that the key characteristics of the evolutionary dynamics in this framework are similar to those of the simpler model, indicating that reducing the antigenic space to one-dimension is indeed a reasonable approximation that produces robust insights.

Deterministic Model

We consider an extension of the model proposed by Andreasen and Sasaki (2006), hereafter denoted the AS-model. This framework focuses on the seasonal dynamics of influenza to separate the epidemiological and evolutionary timescales. The epidemiological dynamics are expressed in a continuous time structure within a single transmission season. The evolutionary dynamics are expressed through a discrete time structure. Time is divided into a sequence of consecutive seasons and the host

population is classified according to the most recent season in which infection occurred. Within any given season the antigenic distance between viral genotypes in the same clade is assumed to be small relative to the distance between clades or the distance between genotypes in different seasons. The system is then simplified by representing the whole collection of genotypes making up a clade as a single 'strain'. In temperate regions multiple introductions seed epidemics of antigenically distinct clades in each transmission season. Diversity is replenished each season from an extensive global gene pool but there is little positive selection over the course of the epidemic (Holmes et al. 2005; Nelson et al. 2006, 2008). Therefore the antigenic type of each clade is assumed to evolve at a constant rate between seasons but remain static within any given season.

At the beginning of each season a mutant strain with a fixed antigenic divergence from the ancestral strain in the previous season founds an epidemic in the host population. The epidemiology of the strain follows the standard SIR model, but the infectivity of the virus depends on host cross-immunity due to past infections. Cross-immunity is modeled as an exponentially decaying function of the time since last infection. At some point within the same season a second strain with fixed divergences from the ancestral and sibling strains is introduced. In the AS-model, the second strain is only introduced when the epidemic of the founder strain has finished. Here we also consider the impact of introducing the second strain during the founder epidemic. Persistence of both strains is a necessary condition for the establishment of a new antigenic branch. We are mainly interested in the conditions that prevent such co-existence and may thus lead to a slim phylogenetic tree.

As in the AS-model, let S_k denote the fraction of hosts whose most recent infection occurred *k* season ago, and have not yet been infected in the current season. Let I_k denote the fraction of hosts that are currently infected, and whose last previous infection occurred *k* seasons ago. Similarly, let R_k denote the fraction of hosts that have recovered from infection in the current season and whose last previous infection occurred *k* seasons ago. For simplicity, the total number of hosts is assumed to be constant ($\sum_j (S_j + I_j + R_j) = 1$) and there is no birth, death, or immigration during the epidemic period. The infectivity of the strain in an infected host is assumed to depend on the number of years since the host was last infected, *k*, according to e^{-ck}. Here *c* is a

constant contact rate and τ_k ($0 \le \tau_0 < \tau_1 < \cdots < 1$) is an increasing function describing the strength of cross-immunity. With these assumptions, the differential equations that describe changes in S_k and I_k in a season are:

$$\begin{aligned} S_k' &= -\lambda S_k, \\ I_k' &= \lambda S_k - \gamma I_k, \\ R_k' &= \gamma I_k, \\ \lambda &= c \sum_k \tau_k I_k, \end{aligned} \tag{1}$$

where the prime ' denotes the time derivative d/dt, λ denotes the force of infection and γ is the recovery rate. As in the AS-model, we assume the following functional form for the cross-immunity:

$$\tau_k = 1 - \alpha^k. \tag{2}$$

Here, α describes how the strength of cross-immunity decays after one season. The cross-immunity decays exponentially with the number k of seasons since the last infection, as shown in Figure 1 for different values of α. We assume that among the past infection events, the most recent infection determines the strength of cross-immunity against the currently circulating strain. Rescaling time in units of the average duration of infection $1/\gamma$, yields

$$\begin{aligned} S_k' &= -\lambda S_k, \\ I_k' &= \lambda S_k - I_k, \\ R_k' &= I_k, \\ \lambda &= r \sum_j \tau_j I_j, \end{aligned} \tag{3}$$

where $r = c/\gamma$ is the basic reproductive rate, the expected number of secondary infections from a single host infected with a particular strain when the rest of the host population has no immunity to any strain.

Let $S_k^p(\infty)$ be the density of the hosts still uninfected at the end of season p whose most recent infection occurred k seasons ago, and $R_k^p(\infty)$ be the corresponding quantity for the hosts infected and recovered in season p. Then the initial condition of the host population at the start of season p+1 is expressed in terms of the state at the end of season p by:

$$S_1^{p+1}(0) = \sum_{k=1} R_k^p(\infty)$$
$$S_{k+1}^{p+1}(0) = S_k^p(\infty) \quad (k \geq 1) \tag{4}$$

The epidemic dynamics in the year $p+1$ are then described by (3) where the superscripts to designate the year are dropped for notational simplicity.

We now expand the AS-model to evaluate how the extent to which two strains co-circulate within the same epidemic season affects the evolutionary dynamics in terms of the establishment of novel antigenic branches. The immune profile of the host population becomes more complex. To incorporate the immune interaction between co-circulating strains we label the strain present at the start of the season A, the strain emerging at some later point B, fix the strength of partial cross-immunity α and constant contact rate c to be the same for both strains and assume that strain A has been circulating for many seasons but strain B first reaches detectable prevalence in season T. Following the AS-model, we assume that both strains A and B are first present at very low prevalence at the end of season $T-1$. Therefore, when they reach detectable prevalence, in season *T*, the antigenic distance between strains A and B is equal to the antigenic distance associated with two seasons in the one strain model. If there are multiple previous infections only the strongest partial cross-immunity is assumed to be effective.

Inter-pandemic influenza subtypes generally circulate for several decades, undergoing antigenic drift throughout this period. The H3N2 subtype currently responsible for the majority of seasonal influenza infections has circulated since 1968 (Kilbourne, 2006) and it is reasonable to assume that the epidemiological dynamics have settled to a stable pattern. The initial immune profile of the population at the start of season *T*, in terms of the length of time since the most recent infection, is found from this steady state. The population is then challenged with a new strain, A, at the start of the Tth season. Later in the same season the population is challenged with another new strain, B. Thereafter, the density of hosts infected with these strains is recorded. The population is now categorized into 9*k* states, susceptible (*S*), infected (*I*) and recovered (*R*) for each strain A and B with the most recent previous infection experienced *k* seasons ago. For example, the proportion of hosts currently infected with strain A, recovered from infection in the current season with strain B and, asides from the current

season, last infected *k* season ago is given by IR_k. The rate of change of each host state is described by the differential equation system:

$$\begin{aligned}
SS_k' &= -(\Lambda_A + \Lambda_B)SS_k, \\
IS_k' &= \Lambda_A SS_k - IS_k - \nu\Lambda_B IS_k, \\
RS_k' &= IS_k - \nu\Lambda_B IS_k, \\
SI_k' &= \Lambda_B SS_k - SI_k - \nu\Lambda_A SI_k, \\
II_k' &= \nu(\Lambda_A SI_k + \Lambda_B IS_k) - 2II_k, \\
RI_k' &= \nu\Lambda_B RS_k + II_k - RI_k, \\
SR_k' &= SI_k - \nu\Lambda_A SR_k, \\
IR_k' &= \nu\Lambda_A SR_k + II_k - IR_k, \\
RR_k' &= RI_k + IR_k,
\end{aligned} \tag{5}$$

where the parameter ν represents the proportional susceptibility reduction due to temporary non-specific cross-immunity. Ferguson et al. (2003), Tria et al. (2005) and Andreason and Sasaki (2006) all note that it is hard to produce a phylogenetic tree with the shape characteristic of influenza without this factor, unless the basic reproductive ratio is close to 1. Here, $0 \le \nu \le 1$ and the effect of temporary non-specific immunity becomes smaller as ν becomes larger. This immunity is only thought to persist for 3-4 months so is not carried over to the next season. Note that co-infection with both strains can occur. However, the II compartment is expected to be very small, and unlikely to play a significant part in the dynamics, because the duration of infection is short and hosts infected with one strain immediately gain non-specific partial immunity to all other strains for the remainder of the season.

The forces of infection of strains A and B, Λ_A and Λ_B, are given by

$$\begin{aligned}
\Lambda_A &= \rho\Big(\sum_{k=1} \tau_k(IS_k + II_k + IR_k) + \tau_0(IS_0 + II_0) + \tau_2 IR_0\Big), \\
\Lambda_B &= \rho\Big(\sum_{k=1} \tau_k(SI_k + II_k + RI_k) + \tau_0(SI_0 + II_0) + \tau_2 RI_0\Big),
\end{aligned} \tag{6}$$

Here $\rho = c/\gamma$ is the basic reproductive rate, the expected number of secondary infections from a single host infected with a particular strain when the rest of the host population has no immunity to any strain. The suffix $k = 0$ indicates hosts that have

never been infected prior to the current season. The proportional reduction in infectivity due to partial cross-immunity of hosts who are currently infected with strain A, have recovered from an infection with strain B in the current season, but have never been infected prior to the current season (IR_0) is τ_2.

Following Andreasen and Sasaki (2006), we assume that the host population has experienced annual outbreaks of a single constantly evolving virus line (A) for a long time, and hence the fractions s_k of hosts last infected k seasons ago at the onset of season are at steady state. The equilibrium values of s_k at the onset of season are thus given by

$$\hat{s}_k = (1-\phi)\phi^{k-1}, \ (k = 1,2,\ldots), \tag{7}$$

where ϕ is the fraction of hosts that remain susceptible in each year, determined from

$$0 = \rho q(1-\phi) + \log\phi, \tag{8}$$

where $q = \sum_k \tau_k \hat{s}_k = \sum_k \tau_k (1-\phi)\phi^{k-1}$. This follows by considering the equilibrium of (4) noting that $S_k^p(0) = S_{k-1}^{p-1}(\infty) = \hat{s}_k$ and $R_k^p(\infty) = S_k^p(0)\phi = \hat{s}_k\phi$. With the partial cross-immunity function (2) assumed in this paper, $q = \sum_{k=1}^{\infty}(1-\alpha^k)(1-\phi)\phi^{k-1}$ $= 1 - \alpha\phi(1-\phi)/\{\phi(1-\alpha\phi)\}$ and hence (8) can be rewritten as

$$0 = \rho(1-\phi)[1 - \alpha\phi(1-\phi)/\{\phi(1-\alpha\phi)\}] + \log\phi. \tag{9}$$

In order to investigate overlapping epidemics of strains A and B, we introduce strain A at the beginning ($t = 0$) of a season. The initial condition is then

$$\begin{aligned} SS_k(0) &= (1-\varepsilon_A)\hat{s}_k, \\ IS_k(0) &= \varepsilon_A \hat{s}_k, \end{aligned} \tag{10}$$

($k = 1,2,\ldots$) where ε_A is a small positive constant representing the initial fraction of strain A infected hosts, and s_k is the initial fraction of hosts whose last infection was k seasons ago as given by (7) and (9). All other classes are zero at $t = 0$. Some time $t = T_d$ after the epidemic of strain A starts, strain B is introduced and the initial condition for the integration of (2) for $t \geq T_d$ is:

$$\begin{aligned} SI_k(T_d) &= \varepsilon_B SS_k(T_d - 0), \quad SS_k(T_d) = (1-\varepsilon_B)SS_k(T_d - 0) \\ II_k(T_d) &= \varepsilon_B IS_k(T_d - 0), \quad IS_k(T_d) = (1-\varepsilon_B)IS_k(T_d - 0) \\ RI_k(T_d) &= \varepsilon_B RS_k(T_d - 0), \quad RS_k(T_d) = (1-\varepsilon_B)RS_k(T_d - 0) \end{aligned} \tag{11}$$

($k = 1, 2, \ldots$) where ε_B is a small positive constant and the fraction $SS_k(T_d - 0)$, for example, represents the value of $SS_k(t)$ in the limit $t \to T_d$. The other three classes for each k, $SR_k(t)$, $IR_k(t)$ and $RR_k(t)$ are zero at $t = T_d$.

The invasibility of strain B in any given year is determined by the sign of the rate of change of the strain B infected population at time $t = T_d$, that is $I_B'(T_d)$ where $I_B(t) \equiv \sum_k (SI_k(t) + II_k(t) + RI_k(t))$ is the total fraction of strain B infected hosts. Strain B will invade the population and cause an outbreak in that year if $I_B'(T_d) > 0$. We examine how this invasibility is related to the degree of overlap between the epidemics, which is measured by $(T_{ea} - T_d)/T_{ea}$, where T_{ea} is the time from the beginning of the season to the moment when the fraction of hosts infected with strain A falls below a fixed extinction threshold.

The coexistence of two strains in the same season is a necessary condition for branching. Influenza phylogenies, however, show distinct branches coexisting for several years until one forms the trunk of the phylogeny and the others become extinct (Bush et al. 1999). Therefore, we now consider the longer term persistence of branches. We assume that strain B successfully increases in the first season it emerges (*T*) and ask if the progeny of both strains A and B still persist n seasons after season *T*. To determine the invasibility of the progeny of strains A and B in season $T + n$, we must know the degree of partial cross-immunity they experience i.e., the shortest path connecting the current strain and the strains responsible for any previous infections along the phylogenetic tree as shown in Figure 2. More specifically, we need to know not only the number of seasons k before *T* that the host has last infected, but also the infection history after season *T* in terms of the progeny of strains A and B. Let a (b) be the number of seasons since the host was *last* infected by the progeny of strain A (B). Let f_a (f_b) be the number of seasons after *T* since the host was *first* infected by the progeny of strain A (B) (see Figure 2(a)). The infectivity $c\tau_{k,a,b,f_a,f_b}$ of strain A infected hosts depends on k, a, b, f_a, and f_b. The entries τ_{k,a,b,f_a,f_b} of Table 1 show the infectivity to the progeny strains of A and B in the year $T + n$ for the hosts with state

$\{k,a,b,f_a,f_b\} = \{+,0,+,0,+\}$ i.e. those who were last infected k years ago at the onset of the season T, have not been infected by any progeny of strain A since then $(a = f_a = 0)$, and have been infected at least once by progeny of strain B $(b, f_b > 0)$. The infectivity $\tau^{A,n}_{k,a,b,f_a,f_b}$ of the progeny of strain A is determined by the most antigenically similar strain i.e. the smaller of $1-\alpha^{n+k}$ and $1-\alpha^{2n+2-f_b}$ as shown in Figure 2(b). $\tilde{\tau}^{A,n}_{k,a,b,f_a,f_b}$ is the corresponding quantity when the host has already been infected by the other co-circulating strain in the same year.

Each of the nine host states in the current season is now additionally classified according to infection history k, a, b, f_a, f_b (e.g. $IS_{(k,a,b,f_a,f_b)}$ represents the density of hosts that are currently infected by strain A, have not yet been infected by strain B in the current season and whose infection history with respect to the ancestral strains of A and B is as shown in Fig 2a). The system is described by differential equations extended from (5) in the obvious way, with the forces of infection of strain A and B, Λ_A and Λ_B, given by

$$\begin{aligned}\Lambda_A &= \rho\sum_k\sum_a\sum_b\sum_{f_a}\sum_{f_b}\{\tau^{A,n}_{k,a,b,f_a,f_b}(IS_{(k,a,b,f_a,f_b)} + II_{(k,a,b,f_a,f_b)}) + \tilde{\tau}^{A,n}_{k,a,b,f_a,f_b} IR_{(k,a,b,f_a,f_b)}\},\\ \Lambda_B &= \rho\sum_k\sum_a\sum_b\sum_{f_a}\sum_{f_b}\{\tau^{B,n}_{k,a,b,f_a,f_b}(SI_{(k,a,b,f_a,f_b)} + II_{(k,a,b,f_a,f_b)}) + \tilde{\tau}^{B,n}_{k,a,b,f_a,f_b} RI_{(k,a,b,f_a,f_b)}\},\end{aligned} \quad (12)$$

Coexistence is determined by the sign of the initial growth rate of the second strain to be introduced. For example, if strain A is initially present and strain B is introduced at $T_d > 0$, then the two strains coexist if $I'_B(T_d) > 0$.

Results

In order to understand the coexistence of two strains we the first consider the model in which only one strain circulates in each season (equation (3)). When the dynamics have stabilized, the distribution of the S_k at the beginning of each season corresponds to the time interval between infections of the same host. As shown in Figure 3, when the basic reproductive number ρ becomes larger, the time interval between infections becomes longer.

With this observation regarding the immune profile in mind, we now analyze the model in which two strains may co-circulate in the same season. Figure 4(a) shows how coexistence in the season that strain B first emerges (T) depends on the basic

reproductive rate ρ, the strength of temporary non-specific immunityν, and the degree of overlap between the epidemics of the two strains. The results can be summarized as follows: (i) If two epidemic does not overlap ($T_d = T_{ea}$) coexistence occurs if ν and $\in$ are large. (ii) If the epidemics overlap a little ($T_d > (3/4)T_{ea}$) the result remains the same. (iii) If the epidemics overlap a lot, the two strains always coexist except when v is very small and $\in$ is very large. The observation that epidemics with different influenza strains often do overlap therefore indicates that, in order to prevent branching, the reproductive number $\in$ must be larger than previously suggested, or broad cross-immunity v must be stronger. Since it is known that the basic reproductive number of influenza is relatively small, this suggests that broad temporary cross-immunity is very effective or there are additional factors involved. If the order of emergence is same in seasons T and $T+1$ the condition for continued coexistence in season T+1 is exactly same. If the order of emergence is reversed between seasons T and $T+1$ the way in which coexistence depends on ρ and v remains qualitatively similar but is restricted to a smaller region of parameter space (Figure 4 (b)). In particular, if T_d is high and $\in$ is small coexistence always occurs for any value of ν. Furthermore, the range of values of T_d that result in large changes in the coexistence condition is narrower than when the order of epidemics is the same and the difference between the coexistence regions associated with $T_{ea}/2$ and T_{ea} is almost undetectable.

Figure 5 summarizes the relationship between the sequence of epidemics and the fate of strains when the A and B epidemics in each season overlap ($T_d = (1/4)T_{ea}$) and do not overlap. The solid line shows the boundary for coexistence when the two strains appear in the same order (AB) in both seasons. The broken line shows the corresponding boundary when the two strains appear in the reverse order (BA) in the second season. If there is no overlap between the two epidemics the result agrees with the analysis of Andreasen and Sasaki (2006). If the two epidemics overlap, the region of the $\rho - v$ parameter space in which strain B excludes strain A is wider when the order of epidemics is reversed between seasons. The effect of overlap between the two strains can thus be summarized as follows: (i) Coexistence occurs over a more extensive region of the r-n parameter space. (ii) If coexistence does not occur strain B is more likely to exclude strain A if the order of appearance is reversed between seasons.

We now consider conditions for coexistence in the season in which strains A

and B appear together for the first time (T) and the following two seasons. There are four possible combinations for the order of epidemics $(AB \to AB \to AB)$, $(AB \to AB \to BA)$, $(AB \to BA \to AB)$ and $(AB \to BA \to BA)$. In season $T+2$, two progeny strains are more likely to coexist than their ancestors due to the increased antigenic distance between them. So if two strains coexist in $T+1$ and the order of epidemics in season $T+2$ is the same as $T+1$, ($(AB \to AB \to AB)$ or $(AB \to BA \to BA)$), coexistence will always continue. If, however, the order of appearance is reversed between seasons $T+1$ and $T+2$, coexistence becomes more limited (Figure 6). Thus, reversal of the order of epidemics between seasons reduces coexistence in the same way as was observed when only seasons T and $T+1$ were considered. Phylogenetic analysis of data from New York State did not find any clear pattern in the order that strains appear from one season to the next (Nelson et al. 2006) suggesting that variation is extensive. Therefore, variation in the order that strains appear is expected to moderate some of the effects of overlapping epidemics and is likely to be a factor in the prevention of branching.

Individual-based simulation

In the differential equation based model discussed so far the time scale of the epidemic is separated from that of the drift process. The main conclusion of our analysis was that two strains are more likely to coexist if there is a shorter time lag between their appearance and hence a greater overlap between their epidemics. Branching may be initiated if two strains appear at a similar point of the season. However, it may be subsequently terminated if the order in which these strains appear varies in later seasons. We now re-examine these conclusions using an individual-based model that simulates the epidemic and drift processes on the same time scale. Whereas the differential equation model is based on the approximation of constant antigenic change in each season, we now model mutation explicitly and only assume that the antigenic distance associated with each mutation is constant.

We consider a host population of $N = 10^5$ individuals and record the immune state of each host with respect to each virus strain. The probability that a host susceptible to strain A becomes infected is

$$\Lambda_A = \rho \sum_{x \text{ infected with A}} \tau_{x,A} / N, \qquad (13)$$

where the summation is over all hosts, *x*, infected with strain A and $\tau_{x,A}$ is the reduced infectivity of strain A in host *x* due to partial cross-immunity, $\rho = c/\gamma$ is the basic reproductive rate, $N = 10^5$ is total host population size, *c* is a constant contact rate and γ is the recovery rate. In order to determine the strength of partial cross-immunity, we need to determine the antigenic distance between two strains. Here we assume this is equal to the Hamming distance. We consider an epitope consisting of ten amino acid residues (loci) and assume each locus has two variants, 0 or 1. The antigenic distance between two strains is then given by the number of loci with different values. For each infected host, one locus of the infecting strain switches value due to mutation with probability μ. Denoting the infectivity reduction rate associated with one mutation by α, the Hamming distance between strains A and B by $d(A,B)$ and assuming only the strongest partial cross-immunity from all past infections is relevant,

$$\tau_{x,A} = \min_{B|\text{x recoverd from B}} (1-\alpha^{d(A,B)}) \quad . \tag{14}$$

Infected hosts recover with probability γ and gain complete temporary immunity to all strains, which lasts an average of 1/5 of a year. The probabilities of birth and death are equal, and newborn hosts are susceptible to all strains. Initially ten hosts are infected with the same strain and susceptible to all other strains while the remainder of the population is susceptible to all strains. The system was iterated using a continuous time Markov process.

Figure 7 shows a phylogenetic tree produced by this model. With temporary non-specific immunity the phylogenetic tree shows an approximately linear shape despite rapid turnover of antigenic strains, justifying our assumption that the viral population is nearly monomorphic in each year and escape mutations constantly accumulate . As with the differential equation model, we now focus on the coexistence of a mutant strain M and its immediate progenitor P. We define M and P to be coexistent if they are both present in the population when another mutation occurs in M. This definition rules out situations in which small outbreaks of P occur by chance even though sustained coexistence is not possible.

Using this model, we tested whether the lag between the appearance of strains P and M is correlated with their coexistence. Figure 8 shows the distribution of the number of mutant strains that coexist with their progenitor P when the lag between

their appearance is T_d. This sampling distribution is compared with a theoretical distribution for the expected number of coexisting strains when the probability of coexistence is independent of T_d and given by

$$F_0 = \frac{\sum_{T_d=0}^{\infty} M_g(T_d)}{\sum_{T_d=0}^{\infty} M(T_d)} \tag{15}$$

Here $M(T_d)$ denotes the number of strains M for which the appearance lag relative to P is T_d and $M_g(T_d)$ denotes the number of strains that have an appearance lag relative to P of T_d and coexist with P. The Kolmogorov-Smirnov test at the critical level 0.01 rejects the null hypothesis that the sampling distribution corresponds to the theoretical distribution. Hence appearance times are correlated with coexistence. Figure 9 shows the relationship between the lag in the appearance time of P and M (T_d) and the probability of coexistence. Spearman's rank-correlation coefficient between the length of the lag and the coexistence probability is -0.4180821 (p-value < 0.01). We conclude that the key dynamics of the deterministic model based on assumption of continuous, linear antigenic divergence are in good agreement with the stochastic model based on a high dimensional antigenic space. If the lag between the appearance of two strains is shorter then they are more likely to coexist. Overlapping epidemics facilitate branching.

Discussion

We have developed a model for influenza evolution over discrete transmission seasons to examine the impact of emergence time and epidemic overlap on the coexistence of antigenically divergent strains and assess the implications for evolutionary branching. Previous work based on non-overlapping epidemics has shown that maintaining the slim antigenic phylogeny of seasonal influenza is likely to require a relatively high basic reproductive number and strong temporary broad immunity. We have shown that if epidemics overlap an even higher basic reproductive number or stronger temporary immunity are required to prevent branching although variation in the order in which strain appear over several seasons may moderate these constraints. We have also shown that these results arise in both a deterministic model with a basic

antigenic space and a stochastic model with a high dimensional antigenic space.

A new branch is established when two distinct strains emerge and coexist. When two strains appear in the same season coexistence is determined by the survival of the second strain and cross-immunity means that hosts infected with, or recovered from, the first strain are difficult for the second strain to re-infect. The key parameters that determine coexistence, therefore, are the decay rate in the strength of partial cross-immunity after one season α, the basic reproductive rate ρ, the proportional reduction in the force of infection due to temporary non-specific immunityν, and the appearance time of the second strain T_d. The role of α and $\nu$is easy to understand as these parameters determine partial cross-immunity and temporary non-specific immunity directly. The role of T_d and ρ, however, is indirect as these parameters determine the immune profile of the host population. A larger value of the basic reproductive rate ρ reduces the time between infections (Figure 3). Given that partial cross-immunity decays with each passing season, and is almost absent after about five seasons, the fraction of hosts who benefit from partial cross-immunity is larger when ρ is larger. In addition to reducing the time between infections, larger values of the basic reproductive rate increase the magnitude of epidemics as shown by S_1 in Table 2. So ρ affects both the fraction of hosts infected and the time between infections. Increasing the time lag between the appearance of each strain (T_d) means that larger values of ρ, or smaller values of ν, are required for coexistence, as Figures 4 and 6 show. This happens because, if the second strain emerges later, a larger fraction of the host population have immunity due to infection with the first strain.

The sequence in which strains appear is also important for coexistence over two seasons. If the sequence of appearance is the same in seasons *T* and *T*+1, continued coexistence is more likely than if the sequence is reversed between seasons (Figure 4). In order to understand this phenomenon, we focus on the case in which the sequence is reversed. In season *T*, strain A emerges first and strain B is suppressed due to host immunity. Hence the number of hosts infected with strain B is small, and so the number of hosts acquiring complete immunity to strain B is also small. This small epidemic may, however, be a herald wave (Glezen et al. 1982), because if strain B appears first in season *T*+1, host immunity is weak and a large strain B epidemic follows. The host immunity arising from this epidemic then suppresses the prevalence of strain A, possibly driving it to extinction. When two epidemics overlap, the exclusion of the

preexisting strain by a strain newly established in a herald wave is much more likely to occur (Figure 5). Once two strains succeed in coexisting it becomes more likely in subsequent seasons, although the extent of potential coexistence is always reduced by a reversal in the order of appearance between seasons.

The key result of both the differential equation based model and the individual based model is that strains are more likely to coexist if the difference between their appearance times is smaller. This conclusion offers important insight into the timing of the emergence of novel influenza strains. For the individual based model, the sampling distribution shown in Figure 8 corresponds to non-neutral evolution whereas the theoretical distribution corresponds to neutral evolution. Here, the degree of overlap between epidemics can also be interpreted as the time at which a mutant emerges from a circulating strain. The peak of the sampling distribution is earlier than that of the theoretical distribution indicating, in agreement with the analysis of Boni et al. (2006), that host immune selection causes excess antigenic drift and most of this drift occurs in the earlier part of each influenza season.

Genetic analysis of H3N2 and H1N1 isolates collected in the United States over the last decade show that there are multiple introduction events each season and several antigenically distinct clades may co-circulate (Nelson et al. 2006, 2007, 2008). Here we have shown that the extent of overlap between the epidemics associated with these clades is an important factor in determining whether or not a new antigenic branch is established, and persists. Clades that appear, by mutation or introduction, at a similar time are more likely to coexist and so result in a new antigenic branch. However, variation in the order in which these clades appear in subsequent seasons limits co-existence and may be an important factor preventing the persistence of new antigenic branches. Analysis of H1N1 epidemiological data has shown that the mutant or clade that emerged earliest in the influenza season caused a major epidemic whilst clades emerging later caused much smaller outbreaks (Nelson et al. 2008). Correspondingly, in our model, strains that emerge when an epidemic of another strain is already well underway are unlikely to lead to significant co-circulation or the establishment of new antigenic branches. This insight suggests that tracking and predicting the antigenic evolution of influenza virus may be improved by focusing attention on the early stages of epidemics.

References

Adams, B. & Sasaki, A. (2007). Cross-immunity, invasion and coexistence of pathogen strains in epidemiological models with one-dimensional antigenic space. *Mathematical Biosciences* 210:680-699.

Adams, B & Sasaki, A (2009). Antigenic distance and cross-immunity, invasibility and coexistence of pathogen strains in an epidemiological model with discrete antigenic space. *Theor. Popul. Biol.* In press.

Andreasen, V. (2003). Dynamics of annual influenza A epidemics with immuno-selection. *J. Math. Biol.* 46: 504-536.

Andreasen, V., Levin, S. and Lin, J. (1996). A model of influenza A drift evolution. *Z. Angew. Math. Mech.* 76: 421-424.

Andreasen, V., Lin, J., and Levin, S. (1997). The dynamics of cocirculating influenza strains conferring partial cross-immunity. *J. Math. Biol.* 35: 825-842.

Andreasen, V. & Sasaki, A. (2006). Shaping the phylogenetic tree of influenza by cross -immunity. *Theor. Popul. Biol.* 70: 164-173.

Boni, M.F., Gog. J.R. Andreasen. V. & Christiansen. F. B. (2004). Influenza drift and epidemic size: the race between generating and escaping immunity. *Theor. Popul. Biol.* 65: 179–191.

Boni, M.F., Gog J.R., Andreasen V. & Feldman M.W. (2006). Epidemic dynamics and antigenic evolution in a single season of influenza A. *Proc. R. Soc. B.* 273:1307-1316.

Bush, R.M., Fitch, W.M., Bender, C.A. and Cox, N.J. (1999). Positive Selection on the H3 Hemagglutinin Gene of Human Influenza Virus A. *Mol. Biol. Evol* **16** 1999b 1457–1465.

Ferguson, N.M., Galvani A.P. & Bush R.M. (2003). Ecological and immunological determinants of influenza evolution. *Nature* 422: 428-423.

Glezen, W.P., Couch R.B. & Six H.R. (1982). The influenza herald wave. *Am. J. Epidemiol.* 116: 589-598.

Gog, J. R. & Grenfell. B. T. (2002). Dynamics and selection of many-strain pathogens. *Proc. Natl. Acad. Sci. USA* 99: 17209-17214.

Haraguchi, Y. & Sasaki, A. (1997). Evolutionary pattern of intra-host pathogen antigenic drift: Effect of cross-reactivity in immune response. *Phil. Trans. R. Soc. Lond. B* 352: 11-20.

Holmes, E.C., Ghedin. E., Miller. N., Taylor. J., Bao. Y., St George. K., Grenfell, B. T., Salzberg, S. L., Fraser, C. M., Lipman, D. J., & Taubenberger. J. K. (2005). Whole-genome analysis of human influenza A virus reveals multiple persistent lineages and reassortment among recent H3N2 viruses. *PLoS. Biol.* 3:e300.

Kilbourne, E.D. (2006). Influenza pandemics of the 20th century. Emerg Infect Dis 12: 9-14.

Koelle, K., Cobey, S., Grenfell, B. and Pascual, M. (2006). Epochal evolution shapes the phylodynamics of interpandemic Influenza A(H3N2) in humans. *Science*. 314:1898–1903.

Lin, J., Andreasn. V., Casagrandi. R. and Levin. S. A. (2003). Traveling waves in a model of influenza A drift. *J. Theor. Biol.* 212: 57-69.

Nelson, M.I., Edelman, L., Spiro, D.J., Boyne, A.R., Bera, J., Halpin, R., Sengamalay, N., Ghedin, E., Miller, M.A., Simonsen, L., Viboud, C. & Holmes, E.C. (2008), Molecular Epidemiology of A/H3N2 and A/H1N1 Influenza Virus during a Single Epidemic Season in the United States. *Plos Pathog*. 4: e1000133.

Nelson, M. I., Simonsen, L., Viboud, C., Miller, M. A. and Holmes, E. C. (2007). Phylogenetic analysis reveals the global migration of seasonal influenza A viruses. *Plos Pathog*. 3: e131.

Nelson, M. I., Simonsen, L., Viboud, C., Miller, M. A., Taylor, J., St George, K., Griesemer, S. B., Ghedin, E., Sengamalay, N. A., Spiro, D. J., Volkov, I., Grenfell, B. T., Lipman, D. J., Taubenberger, J. K. and Holmes, E. C. (2006). Stochastic Processes Are Key Determinants of Short-Term Evolution in Influenza A Virus. *Plos Pathog*. 2: e125.

Sasaki, A. (1994). Evolution of antigen drift and switching: Continuously evading pathogens. *J. Theor. Biol.* 168: 291-308.

Sasaki, A. & Haraguchi, Y. (2000). Antigenic drift of viruses within a host: A finite site model with demographic stochasticity. *J. Mol. Evol.* 51: 245-255.

Smith, D.J., Lapedes, A.S., de Jong J., Bestebroer, T.M., Rimmelzwaan, G.F., Osterhaus, A.D.M.E. and Fouchier, R.A.M. (2004). Mapping the Antigenic and Genetic Evolution of Influenza Virus. *Science*. 305, 371–375.

Tria, F., Lassing, M., Peliti, L. & Franz, S. (2005). A minimal stochastic model for influenza evolution. *J. Stat. Mech. Theor. Exp.* P07008.

Figure legends

Figure 1: Decay in partial cross-immunity with time. The horizontal axis is the number of seasons *k* that have elapsed since the most recent infection. The vertical axis is the reduction in the force of infection due partial cross-immunity, $\tau = 1 - \alpha^k$. The parameter α determines the decay in partial cross-immunity after one season has elapsed.

Figure 2: (a) Relationship between the season in which strains circulate relative to the first potential branch point in season *T* and the antigenic distance between them, indicating the definition of k, a, b, f_a, and f_b. (b) Cross-immunity is determined by the strain most antigenically similar to the one circulating in the current season $T + n$ i.e. the smaller of $1 - \alpha^{n+k}$ and $1 - \alpha^{2n+2-f_b}$.

Figure 3: The relationship between the basic reproductive rate ρ and the mean time interval between of infections of same host when there is only one strain and it has reached equilibrium. Error bars denote standard deviation.

Figure 4: Conditions for coexistence of strains A and B in terms of parameters ρ and ν for different lags between the appearance time of the strains, expressed as a proportion of the total epidemic duration T_{ea} (a) The sequence of epidemics is the same in seasons *T* and *T*+1. (b) The sequence of epidemics is reversed between seasons *T* and *T*+1. The two strains coexist in the regions above the solid lines, one strain is excluded in the regions below the lines, The initial number of infections when each strain appears is $\varepsilon_A = \varepsilon_B = 10^{-6}$. The extinction threshold for each strain is $\sum_k I_k = 5 \times 10^{-7}$.

Figure 5: Relationship between the sequence of epidemics and the fate of the progeny of strains A and B when epidemics overlap ($T_d = (1/4)T_{ea}$) and do not overlap. The solid line is the boundary condition for coexistence if the sequence of epidemics is same in seasons *T* and *T*+1. The broken line is the boundary if the sequence of epidemics is reversed between seasons. The diagrams show which strains persist. • indicates persistence, × extinction. In region (i) the two strains coexist. In region (iii) one strain is

excluded. In the region between the solid and broken lines (ii), the outcome depends on the order of appearance. If strain A appears first in season T+1 there is coexistence but if strain B appears first in season T+1 strain A will be driven to extinction.

Figure 6: Conditions for coexistence of strains A and B in terms of parameters ρ and ν for different lags between the appearance time of the strains. The two strains coexist in the region above the solid line. One strain is excluded in the region below the line, (a) The sequence of epidemics in season T+1 and T+2 is $(AB \to AB \to BA)$. (b) The sequence of epidemics in season T+1 and T+2 is $(AB \to BA \to AB)$.

Figure 7: Phylogenetic tree resulting from a 100 year simulation using the individual based model. Strains that caused less than 2000 infections and did not produce mutants have been excluded. Each branch shows a strain created by one site mutation. Basic reproductive ratio ρ is 3.9968, host population size is 10^5, mutation rate $\mu = 0.0005$, mean duration of protection due to temporary non-specific immunity is $1/5$ year. During temporary immunity hosts cannot be infected by any strain. Initially all of the host population is susceptible to all strains except for 10 hosts infected with the same strain.

Figure 8: The number of progeny strains that emerged the relative lag T_d after the appearance of their ancestors, and coexisted with the ancestors until they leave the next progeny strain, where the lags are scaled in units of the duration of the ancestral strain epidemic. Black bars: the observed distribution from the individual based model; gray bars: the theoretical distribution when there is no correlation between the probability of coexistence and the appearance time. Earlier emerging progeny strains are more likely to coexist with their ancestral strains than random expectation. See text for the definition of the coexistence between ancestral and progeny strains.

Figure 9: Probability that a mutant strain coexists with its progenitor as a function of the lag between the appearance of the two strains, T_d . Error bars denote standard error. As in Figure 8, this shows that earlier emerging progeny strains are more likely to coexist with their ancestral strains.

Table 1: Relationship between infection history and strength of partial cross-immunity (τ) in season $T+n$. "(not) infected by A(B)" indicates whether or not the host is infected with strain A(B) in the current season. Suffix *k* indicates how many seasons before *T* the most recent infection occurred. Suffix *a* indicates how many seasons before the present, but after season *T*, the most recent infection with strain A occurred. Suffix *fa* denotes how many seasons before the present, but after *T*, the first infection with strain A occurred. Suffixes *b* and *fb* are similarly defined for strain B.

Figure

Figure 1

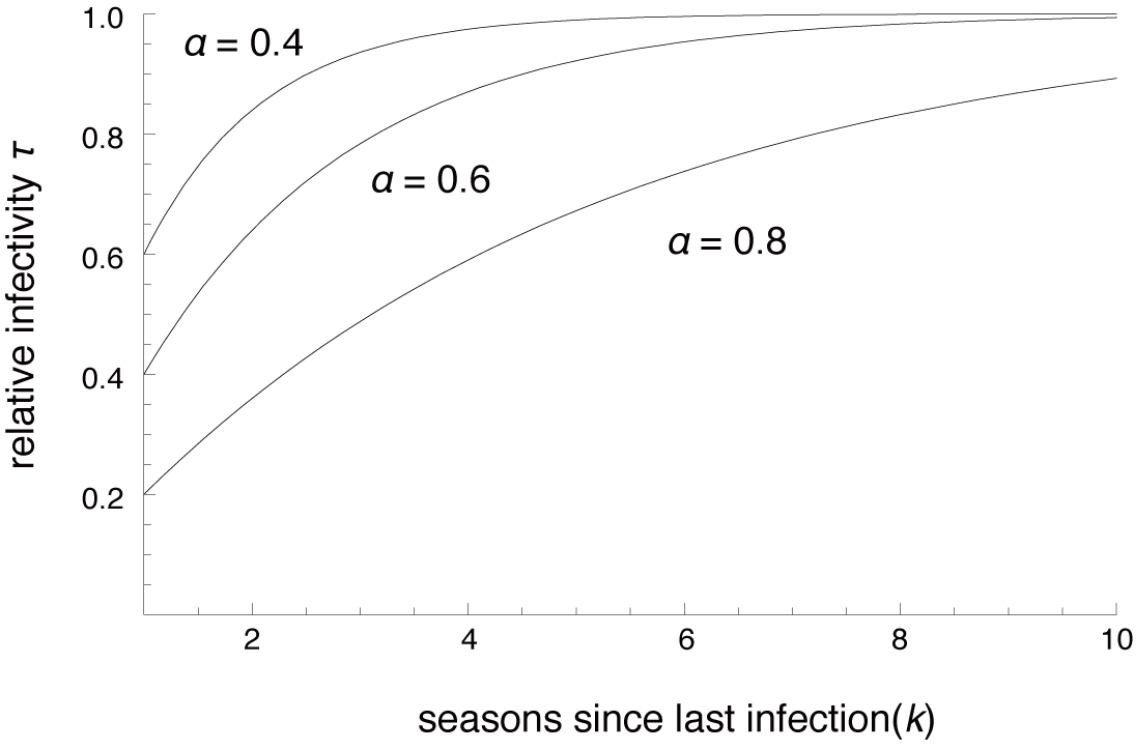

Figure 2

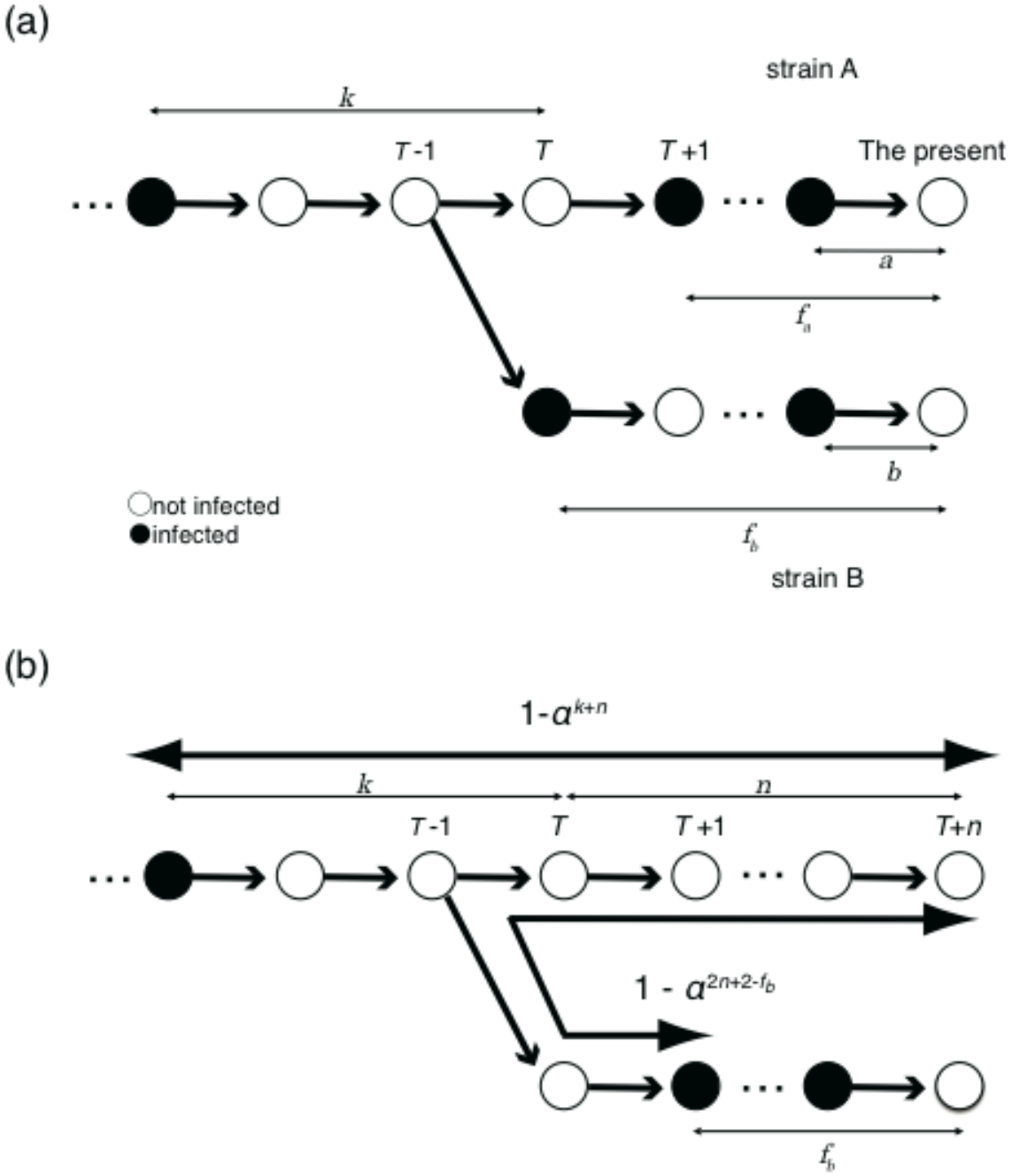
(a)
strain A
k
T-1
T
T+1
The present
a
f_a
b
f_b
not infected
infected
strain B
(b)
$1-\alpha^{k+n}$
k
n
T-1
T
T+1
T+n
$1-\alpha^{2n+2-f_b}$
f_b

Figure 3

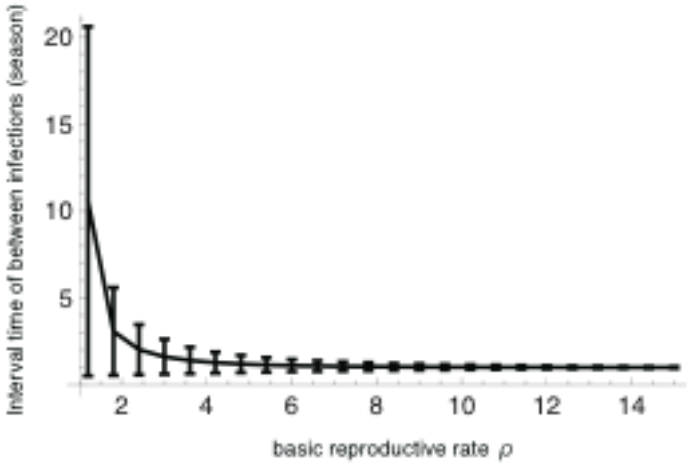
Interval time of between infections (season)
20
15
10
5
2
4
6
8
10
12
14
basic reproductive rate ρ

Figure 4

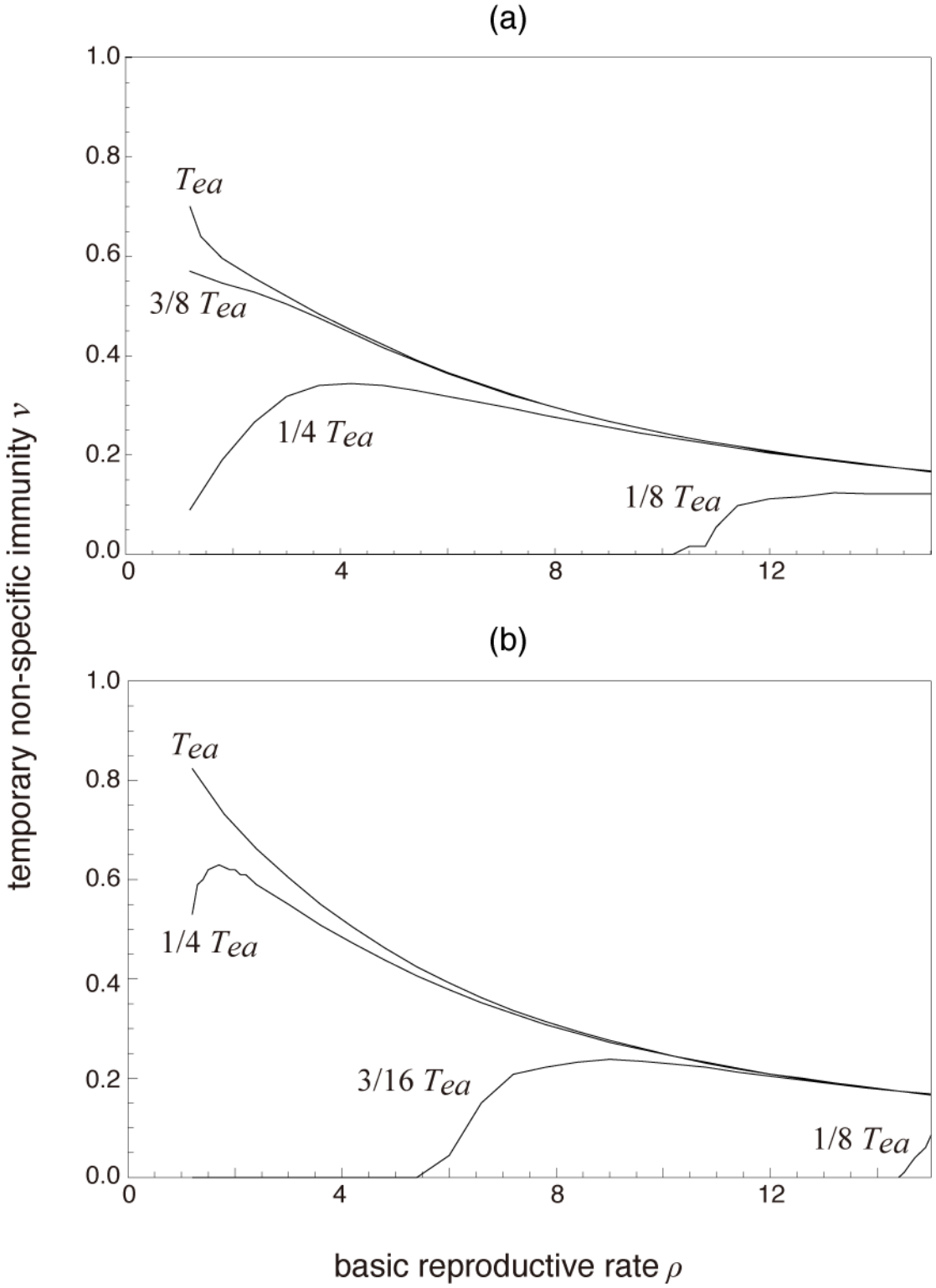
(a)
1.0
0.8
0.6
0.4
0.2
0.0
0
4
8
12
Tea
3/8 Tea
1/4 Tea
1/8 Tea
(b)
1.0
0.8
0.6
0.4
0.2
0.0
0
4
8
12
Tea
1/4 Tea
3/16 Tea
1/8 Tea
temporary non-specific immunity ν
basic reproductive rate ρ

Figure 5

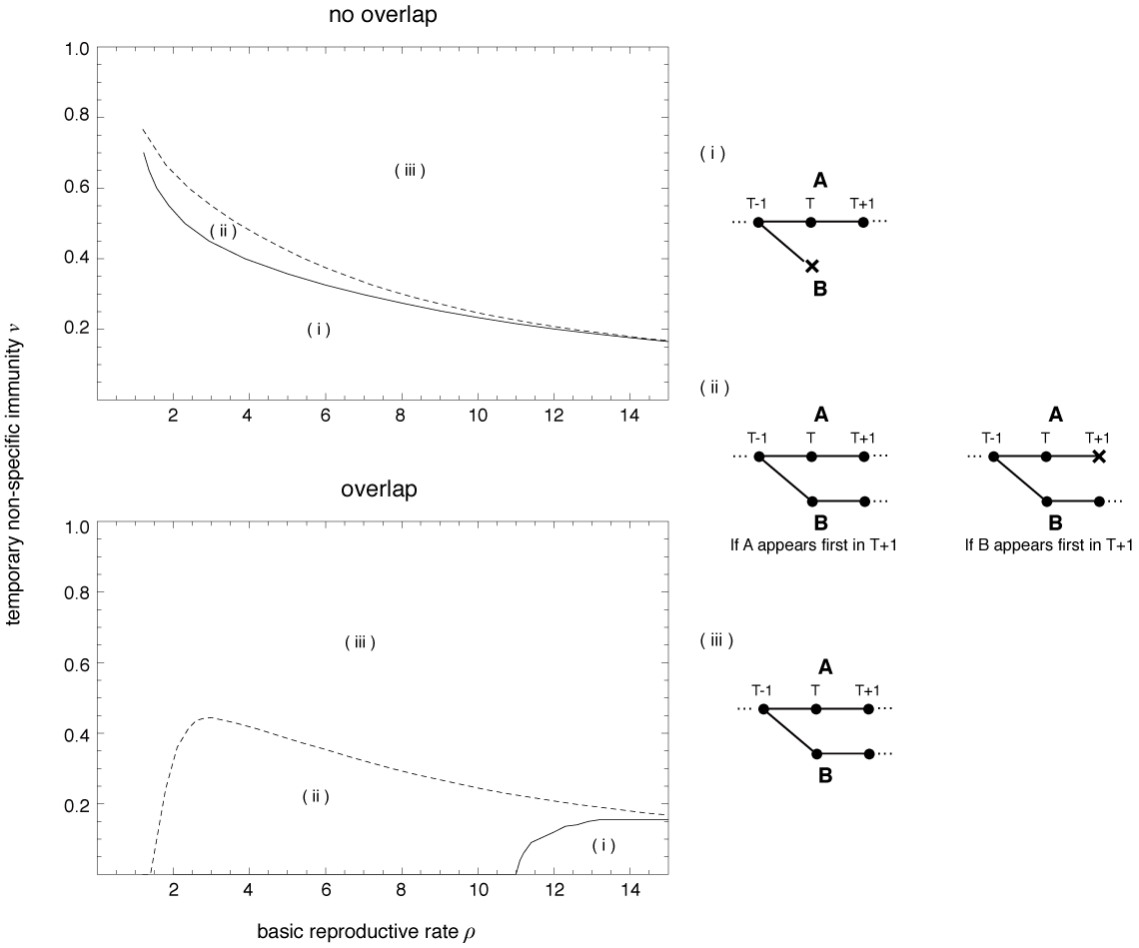
no overlap
overlap
temporary non-specific immunity v
basic reproductive rate ρ
1.0
0.8
0.6
0.4
0.2
2
4
6
8
10
12
14
(i)
(ii)
(iii)
A
B
T-1
T
T+1
If A appears first in T+1
If B appears first in T+1

Figure 6

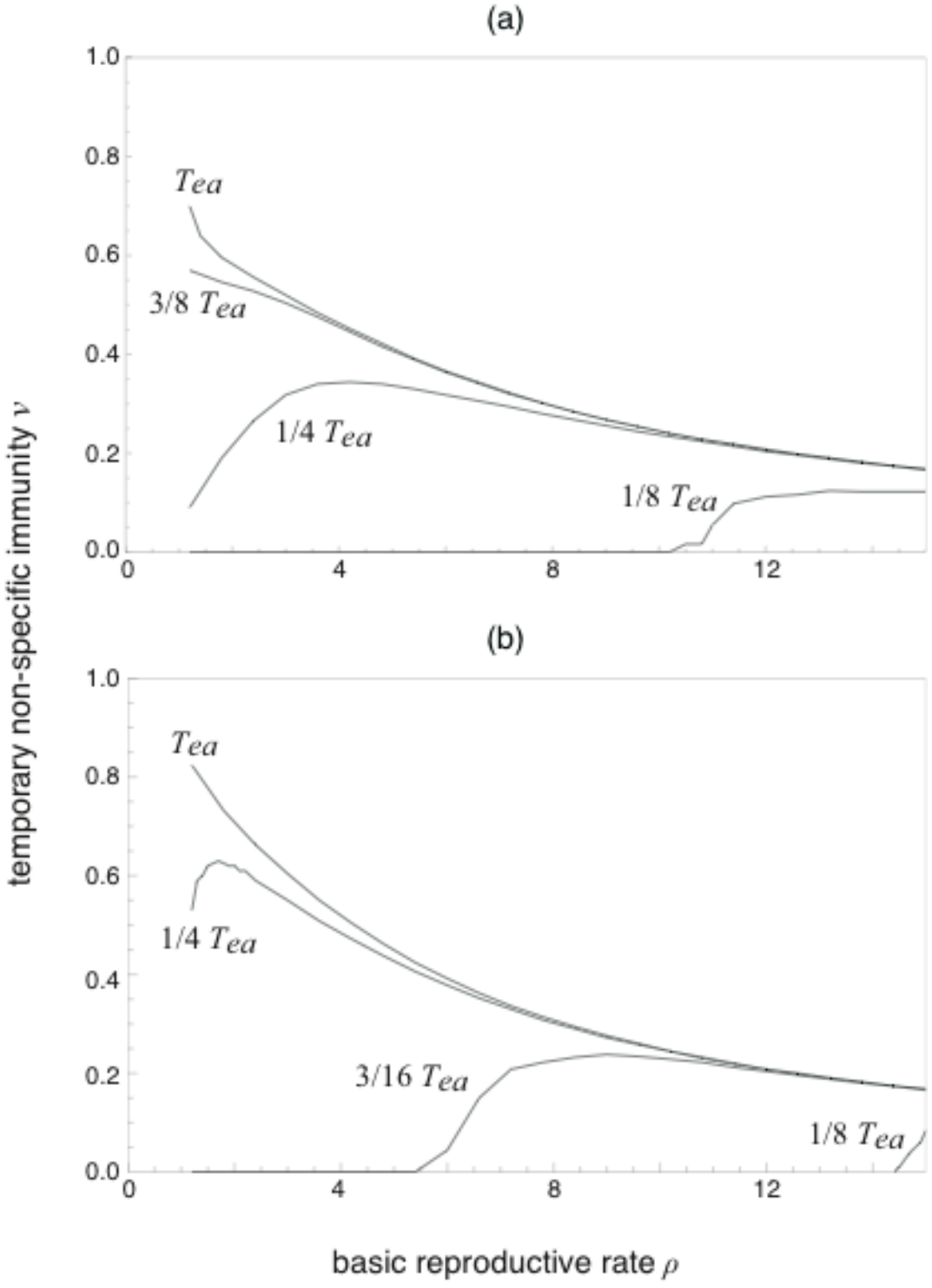
(a)
1.0
0.8
0.6
0.4
0.2
0.0
0
4
8
12
Tea
3/8 Tea
1/4 Tea
1/8 Tea
(b)
1.0
0.8
0.6
0.4
0.2
0.0
0
4
8
12
Tea
1/4 Tea
3/16 Tea
1/8 Tea
temporary non-specific immunity v
basic reproductive rate ρ

Figure 7

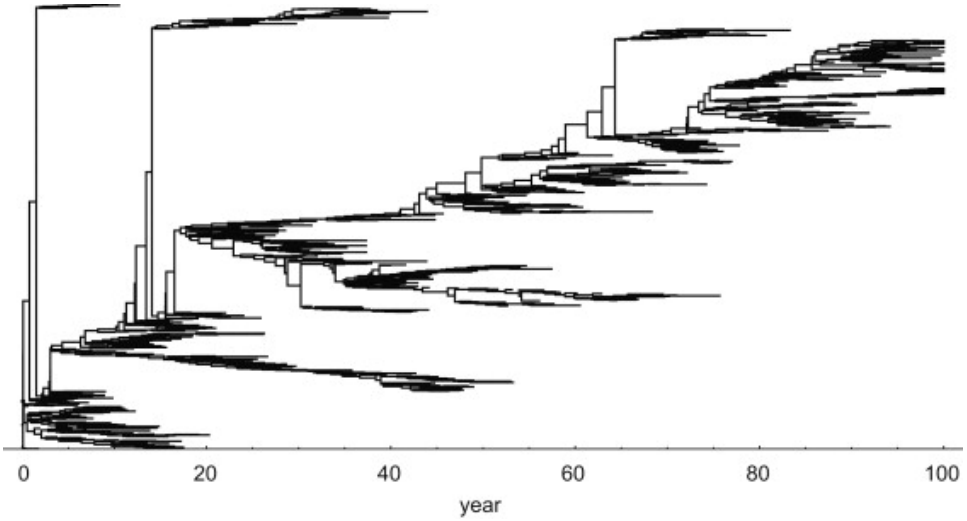

Figure 8

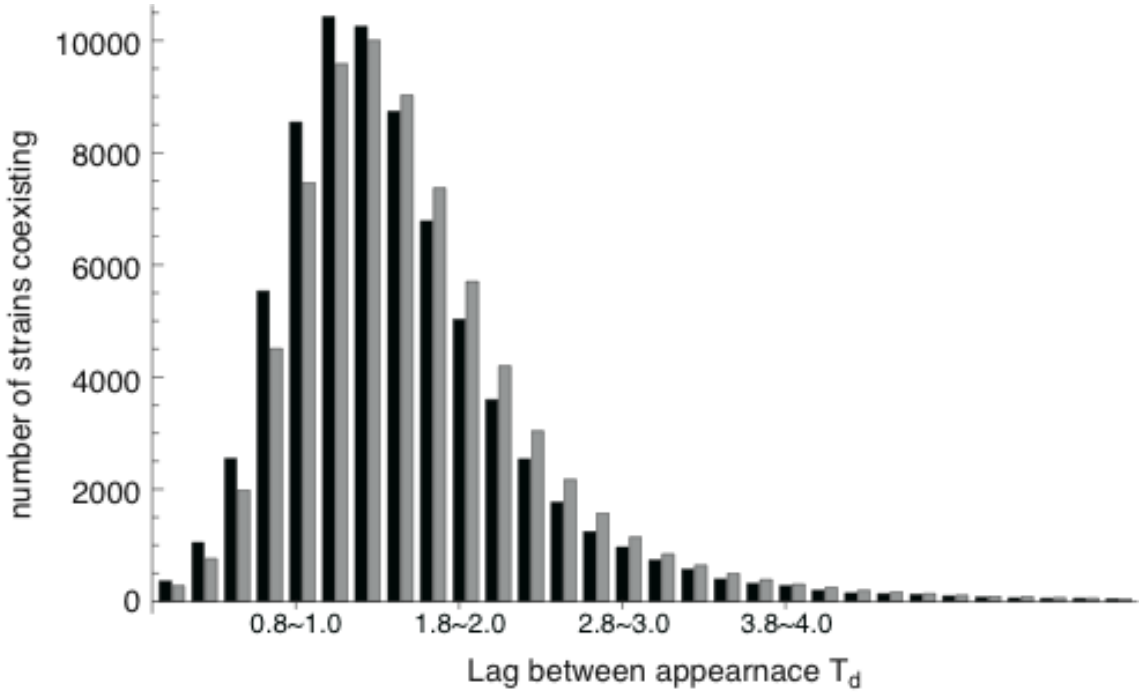

Figure 9

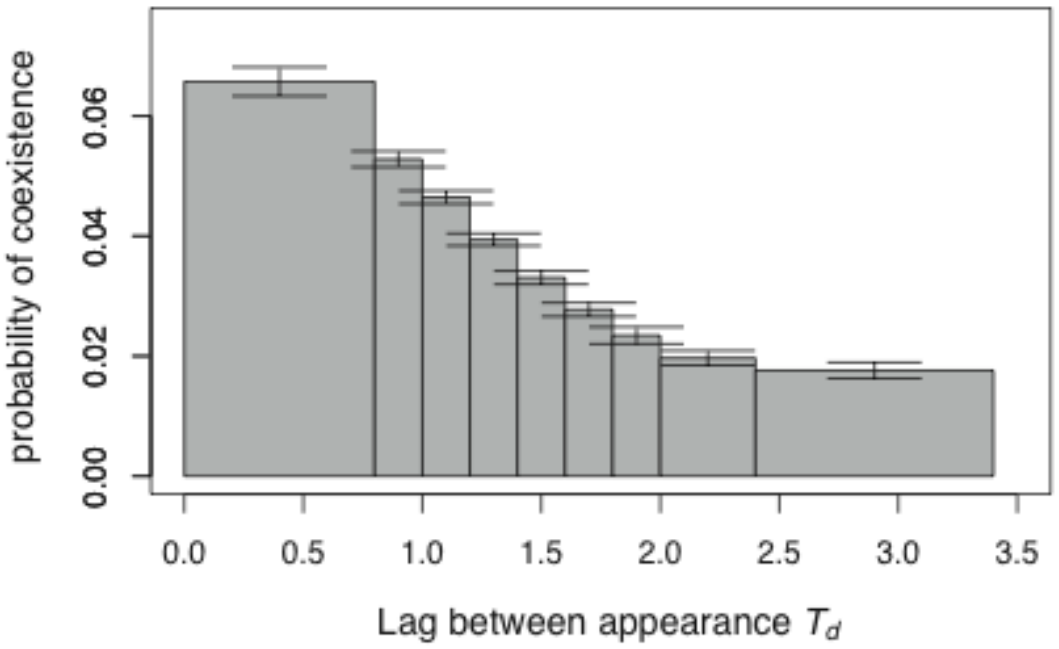
probability of coexistence
0.00
0.02
0.04
0.06
0.0
0.5
1.0
1.5
2.0
2.5
3.0
3.5
Lag between appearance T_d

Table

Table 1

	A	RA	B	RB
$\tau_{(0,0,0,0,0)}$	1	$1-\alpha^{2y}$	1	$1-\alpha^{2y}$
$\tau_{(0,a,0,fa,0)}$	$1-\alpha^{a}$	$1-\alpha^{a}$	$1-\alpha^{2y-fa}$	$1-\alpha^{2y-fa}$
$\tau_{(0,0,b,0,fb)}$	$1-\alpha^{2y-fb}$	$1-\alpha^{2y-fb}$	$1-\alpha^{b}$	$1-\alpha^{b}$
$\tau_{(0,a,b,fa,fb)}$	$1-\alpha^{a}$	$1-\alpha^{a}$	$1-\alpha^{b}$	$1-\alpha^{b}$
$\tau_{(k,0,0,0,0)}$	$1-\alpha^{k+y-1}$	$1-\alpha^{k+y-1}$ (k-1 < y) $1-\alpha^{2y}$ (k-1 >= y)	$1-\alpha^{k+y-1}$	$1-\alpha^{k+y-1}$ (k-1 < y) $1-\alpha^{2y}$ (k-1 >= y)
$\tau_{(k,a,0,fa,0)}$	$1-\alpha^{a}$	$1-\alpha^{a}$	$1-\alpha^{k+y-1}$ (k-1 < y-fa) $1-\alpha^{2y-fa}$ (k-1 >= y-fa)	$1-\alpha^{k+y-1}$ (k-1 < y-fa) $1-\alpha^{2y-fa}$ (k-1 >= y-fa)
$\tau_{(k,0,b,0,fb)}$	$1-\alpha^{k+y-1}$ (k-1 < y-fb) $1-\alpha^{2y-fb}$ (k-1 >= y-fb)	$1-\alpha^{k+y-1}$ (k-1 < y-fb) $1-\alpha^{2y-fb}$ (k-1 >= y-fb)	$1-\alpha^{b}$	$1-\alpha^{b}$
$\tau_{(k,a,b,fa,fb)}$	$1-\alpha^{a}$	$1-\alpha^{a}$	$1-\alpha^{b}$	$1-\alpha^{b}$

Table 2

ρ	S_1	S_2	S_3	S_4	S_5	S_6
1.2	9.48%	8.58%	7.77%	7.03%	6.36%	5.76%
7.5	94.69%	5.04%	0.27%	0.01%	0.00%	0.00%
15.0	99.75%	0.25%	0.00%	0.00%	0.00%	0.00%

Chapter 2

The timing of the emergence of new successful strains in seasonal influenza

The study of this chapter was done in collaboration with Dr. Akiko Ohtsuki and Prof. Akira Sasaki.

Introduction

Influenza viruses rapidly change their antigenicity (antigenic drift), making the vaccination strategy against them very difficult. Forecasting the evolutionary trajectory of influenza antigenicity is therefore quite important to prevent an epidemic. The evolution of influenza is driven by selection due to the change in the host herd immunity, as well as random factors like mutations, demographic stochasticity, and environmental fluctuation. Combined effect of these factors should mold the direction of the evolutionary trajectory. A new viral strain must face not only the immune response directly mounted against it, but also partial cross-immunity due to the past infection of related strains. In addition to the specific immune responses, a newly infected strain must face temporal non-specific immunity raised by the infection of an arbitrary strain. These immune-driven processes should play a key role in the evolution of influenza. The immune response due to earlier infection of a strain would suppress the epidemiological outbreak of other strains emerging later, which would drive the late coming strains to go extinct. This 'mass extinction' of strains, which would be highly successful if it originated in a susceptible population, but not in the population experienced the recent outbreaks of closely related strains, makes phylogenetic tree of influenza slender (Andreasen et al., 1997; Ferguson et al., 2003; Koelle et al., 2006; Andreasen and Sasaki, 2006; Omori et al. 2010). The strength of host herd immunity against a new flu strain is determined by how far it is genetically or antigenically distant from the strains the host population experienced in the past. Mathematical models that explicitly take into account the phylogenetic relationship between strains are therefore necessary to understand the evolution of influenza. In this paper, we study the model describing the evolution of antigenic sites of virus that allows the mutation to alter the antigenicity and is exposed to the selection due to host immunity and cross-immunity. We used the mathematical model that described host population dynamics in each host immune classes with each strain, so called multi strain model. Previous studies based on multi strain model have revealed which of possible strains is dominant at equilibrium (Gupta et al., 1996, Minayev and Ferguson, 2009, Recker et al., 2007). We focus on the distribution of the emergence timing, the epidemic peak timing and the epidemic duration of strain which will successfully establish itself in the host population, by extensive simulations of individual based model for the co-circulation of antigenic

strains.

Method

We consider 10^5 host population, and keep track of the immune status of each host individual against each virus strain. Let $H_{x,n}$ denote the immune status of the x-th person against a viral strain *n*,

$$H_{x,n} \in \{0,1,2\}, \tag{16}$$

where the state 0, 1, and 2 respectively means that the host is susceptible to, infected by, and recovered from the viral strain n. We consider the immunity and cross-immunity against a viral strain in term of the infectivity of the strain. For example, the force of infection Λ_A of strain A, or the rate at which a host is infected by strain A, is defined as

$$\Lambda_A = \beta \sum_{x|H_{x,A}=1} \tau_{x,A}, \tag{17}$$

where summation is taken for all the hosts, x, infected by strain A (i.e. with the state $H_{x,A}=1$). β is the transmission rate of virus, constant over strains but has seasonal variation with annual cycle

$$\beta(t) = \beta_0(1 + a\cos(2\pi t)), \tag{18}$$

where β_0 is the mean transmission rate, a is the amplitude of seasonal fluctuation of the transmission rate. $\tau_{x,A}$ is infectivity of strain A reduced by cross-immunity of *x*-th person,

$$\tau_{x,A} = \min_{B|H_{x,B}=2} (1-\alpha^{d(A,B)}). \tag{19}$$

Here we assume that the closer is the antigenic distance $d(A,B)$ between strains A and B, the stronger is the degree immune protection, $\alpha^{d(A,B)}$, by cross immunity, where α is a constant in the range $0<\alpha<1$. The infectivity of a strain A is assumed to be determined by the strongest cross-immunity in all the past infections of *x*th person. This corresponds to take the minimum of infectivity over all the viral strains B that has infected the host x in the past. α is infectivity reduction rate by one mutation.

The antigenic distance $d(A,B)$ is defined as the hamming distance between the epitope sequences of strain A and B. We consider epitope sequence of length ten,

where each site has two alleles 0 and 1. The immunological distance between two strains is determined by the number of unmatched sites in the epitope (hamming distance). Each site changes its allelic states by mutation with the rate μ.

An infected host recovers at the rate γ, and the recovered host gets temporary non-specific immunity. The host in this class is protected from any strain. Temporary immunity is lost at a constant rate ν. For the sake of simplicity, birth and death rates of a host, denoted by u, are assumed to be the same so that the total population is kept constant, and newborns are susceptible to all the strains. The initial condition is that the host population is completely susceptible to any strain except ten host individuals infected by a single inoculated strain with the epitope sequence 00…0. Birth and death of hosts, infection and recovery events, and mutations at antigenic sites of influenza occur randomly with the rates described above (the model is therefore falls into the category of a multi-agent continuous-time Markov chain).

Previous studies revealed that, to realize a slender phylogenetic tree that characterizes of the evolutionary pattern of influenza A virus, the epidemiological parameters must reside in a certain range. Firstly, an intermediate basic reproductive ratio is necessary for a long persistence of viruses by continuously escaping host immune response (Sasaki and Haraguchi 2000). Secondly, for a secure long persistence of slender phylogenetic tree during antigenic drift, sufficiently strong general temporary immunity or suppression of co-infection is necessary (Andreasen and Sasaki 2006, Omori et al. 2010). As we are interested in the long lasting antigenic drift of influenza viruses, we restricted our analysis in the range of epidemiological parameters of cross-immunity and general temporary immunity (β, ν, α and a) so that the viruses succeeded to persists more than 1000 years by continuously evading immune response in the simulation. If co-infection is not suppressed, strong enough general temporal immunity is required (Figure s1), this agrees with Andreasen and Sasaki 2006 and Omori et al. 2010. In the case that co-infection is suppressed, the lineage of virus can persist for a long time even if there is no general temporal immunity. Other parameters are kept constant : γ = 25.0 per year by which the infectious period $1/\gamma$ is set about two weeks, u = 1/50 by which mean host life time is 50 years, and mutation rate per antigenic site per infection event m = 0.001.

Results and Discussion

We first focus on the distribution for the emergence times of new strains in a year observed in our Monte Carlo simulations. The peak time for the generation of new strains in a year was earlier than the time at which the infection rate attained its maximum (Figure 10a). A new strain of virus here is defined as the one having at least one mutation at epitope sites from its direct ancestor. We then focus on a subset of new strains that will later succeed in producing further new strains (Figure 10b-d). We call these strains the second-generation-producing strains. Among a large number of new viral strains generated by mutations in each year, only a small fraction of them could establish themselves in host population (compare the vertical axis of Figure 10a with those of Figure 10b-d). All the other new strains went extinct without showing any detectable increase in the population. As a result the shape of phylogenetic tree became nearly linear, as has been shown empirically in influenza A viruses (Buonagurio et al., 1986, Cox and Subbarao, 2000, Fitch et al., 1991, Fitch et al., 1997, and Hay et al., 2001). The second-generation-producing strains in our simulations thus correspond to the strains constituting the “trunk” of cactus shaped phylogenetic tree of influenza.

Let us now consider the emergence time, the time at which it is generated by mutation, of the second-generation producing strains. The peak times of the emergence of the second-generation-producing strains were earlier than those of all the strains (Figure 10b as compared with Figure 10a). We also studied the peak times of the emergence of the third-generation-producing, and the forth-generation-producing strains. However, there were no clear difference between the peak emergence time of these strains from that of the second-generation-producing strains (Figure 10b-d). This means that, although the success in the production the second generations critically depended on the timing of its emergence in a year, further success in the production of the third or further generations was nearly independent of the emergence time of the strain.

Markedly earlier emergence of successful (the second generation producing) strains in the year among all the new strains was shown over a wide range of parameters (Figure 11). The emergence times in a single epidemic season of the second-generation producing strains were consistently and considerably earlier than the mean emergence times of all the new strains that include those went extinct before increasing in the host population (red, blue, green lines in comparison to black lines in Figure 11).

Although the advanced emergence times of successful strains over the other strains hardly changed with the parameters, they change in accordance with each

epidemiological parameter. The increased mean basic reproductive ratio $\bar{R}_0$ led to earlier peak time of the emergence of all the new strains (Figure 11a). This can be simply ascribed to the classical result of epidemiological model (e.g. Anderson and May 1991) --- an earlier peak of outbreak for a larger basic reproductive ratio. It is interesting to note that for a sufficiently large $\bar{R}_0$, the mean emergence time was set back again due to demoted synchronizations of epidemiological outbreaks by different strains (denoted by larger variances in peak emergence times towards larger $\bar{R}_0$ -- see supporting information for the theoretical explanation for the demoted synchronization with a larger basic reproductive ratio). In the similar vein, the decrease in the degree of cross-immunity (the decrease of α) by a single mutation in antigenic sites led to an earlier peak of emergence (Figure 11b). We also observed that a more strong general temporal immunity (i.e. a longer mean duration of general temporal immunity) led to an earlier peak of emergence (Figure 11c). There was no clear effect of the amplitude a of seasonal fluctuation of transmission rate (Figure 11d).

The reason why the emergence time of successful strain (the second-generation producing strains) was earlier than the other strains can be explained by the advantage of strains emerged in an early stage of epidemic season over the other strains (Omori et al. 2010). An earlier coming strain in an epidemic season suffers less from cross-immunity or temporal immunity mounted by the other strains. Later coming strains, on the other hand, are more heavily suppressed by the cross-immunity of the hosts infected by antigenically similar strains. General temporary immunity also contributes to the advantage of an earlier strain, as in the same vein cross-immunity does. This by no means implies that the strain with the earliest emergence in the season become the major strain of the year; the strains emerging too early must face smaller transmission rates (which is fluctuating seasonally) than in the peak season. There is therefore the optimum timing of the emergence in a year to be successful for the virus, which is much earlier than the peak time of the epidemic, and against which we must be precautious.

We next focus on the time for a strain to reach the maximum infectious population after it emerged. Figure 12 shows that, during the epidemic courses of particular strains, most epidemic peaks were attained around one year after their emergences. This means that, in most cases, the strain that causes an epidemic have already emerged in the last epidemic season, suggesting that we can detect the strain that will become dominant in

the next year by looking in current epidemic season. However, if $\bar{R}_0$ was too large this was no longer the case: there is high probability of failing such prediction. If $\bar{R}_0$ was large, many strains attained their epidemic peaks in the same season they emerged. This means that even at the late stage of epidemic season, it is too early to find the potential dominant strains of the next season if the basic reproductive ratio is large. The other parameters (α, $1/\nu$ and a) made small difference in the fraction of hosts who were infected in the first year the strain emerged. They, however, made big difference in the distribution for the time of infection *after* the second year the strain emerged. The increased infectivity reduction rate α, the prolonged duration of temporal immunity $1/\nu$, and the decreased amplitude of seasonality in transmission rate a, all contributed to reduce the frequency of the hosts that were infected in the second year the strain emerged. Despite these parametric dependencies for the infection timing spectrum after the second year, the *mean* time of infection did not change much by α, $1/\nu$ or a, because they hardly affected the frequency of the hosts who were infected in first year the strain emerged.

This carry-over of epidemic peak of a strain from the season it emerged to the next or later epidemic seasons would be quite important to predict new successful strains. What, then, makes this carrying over? To answer this question we constructed a deterministic model for the epidemics of a single strain in the host population where its immune structure changed with time according to the mean behavior observed in the individual-based model simulation. The epidemic peak timing of the model fitted with, or was self-consistent with, the result of the IBM model (Figure 13). Prohibition of co-infection and addition of general temporal immunity both contributed to carry over the epidemic peak timing of the strains that emerged in early stage of the season.

We also analyzed the dependence of the epidemic duration of the second-generation-producing strain on the parameters ($\bar{R}_0$, α, $1/\nu$ and a). The epidemic duration is defined as the period from the emergence time of the first infectious host to the time when the last infectious host recovered. The results as shown in Figure 14 can be summarized as follows: the epidemic duration increased if $\bar{R}_0$ was increased, and if α and a were decreased. There was, however, no clear effect of general temporal immunity, $1/\nu$, on the epidemic duration.

A larger basic reproductive ratio makes the epidemic duration *shorter* in the SIR model if there were only one strain (i.e. in a standard SIR model) (Figure S2). In

contrast, in the IBM model with many co-circulating strains, the increase in the mean basic reproductive ratio $\bar{R}_0$ led to the increase in the epidemic duration of the second-generation-producing strain (Figure 14a). To understand this discrepancy in the dependence of epidemic duration on $\bar{R}_0$, we focus on the role of competition between co-circulating strains for their hosts. For a larger number of co-circulating strains, we expect more intense competition between them, and hence we expect a smaller peak of epidemic and prolonged epidemic duration by each strain. This was supported by the IBM model. We found that the *total* number of hosts infected in a season increased with $\bar{R}_0$ (Fig S3a), but that the *mean* number of hosts infected by *each* strain *decreased* with $\bar{R}_0$ (Fig, S3c). This is because the "denominator", the number of emerged strains per season, increased *further* than the "numerator", the total number of infected hosts, with $\bar{R}_0$ (compare Fig. S3a with S3b). Similarly, a longer epidemic duration with a smaller α (Figure 14b) suggests that more efficient cross-immunity by a single mutation (i.e. decreased α) led to a more intense competition between co-circulating strains.

The reason why a greater fluctuation in transmission rate (by increased *a*) makes epidemic duration of the second-generation-producing strain shorter (Figure 14d) can also be explained by more intense competition between co-circulating strains. Indeed, the denominator of *mean* number of hosts infected by a particular strain (i.e. the number of strains emerge in a season) increased further than the numerator (i.e. the *total* number of infected hosts) with increasing *a* (Figure S4a and S4b). Rambaut et al. (2008) revealed that the epidemic of influenza A in high latitude region has stronger seasonality than low latitude region, it is suggested that epidemics of each influenza strain in low latitude region should persist longer.

As for general temporal immunity, there was no clear effect on epidemic durations (Figure 14c). This is consistent with the fact that there is no clear difference in the *mean* number of hosts infected by the second-generation-producing strain that emerged in a season for varying $1/\nu$ (Figure S5c). A greater general temporal immunity (i.e. a longer duration of temporal immunity) decreased to the same extent both the total epidemic size and the number of strains emerging per year (Figure S5a and S5b).

The key result of our paper is that the strains that will produce new strains tended to emerge in an early stage of epidemic season, and to reach its maximum number of infected hosts in the next season. Predicting a strain that will become dominant in the next year is usually difficult, but our study suggest that the census of the already

emerged strains has high chances of finding a dominant strain of the next year.

References

Anderson, R. M. & May, R. M. (1991) Infectious Diseases of Humans: Dynamics and Control. Oxford Univ. Press. Oxford.

Andreasen, V. & Sasaki, A. (2006). Shaping the phylogenetic tree of influenza by cross-immunity. *Theor. Popul. Biol*. 70: 164-173.

Andreasen, V., Lin, J. & Levin, S. (1997). The dynamics of cocirculating influenza strains conferring partial cross-immunity. *J. Math. Biol*. 35: 825–842.

Buonagurio, D., Nakada, S., Parvin, J., Krystal, M., Palese, P. & Fitch, W. (1986) Evolution of human influenza A virus over 50 years: rapid, uniform rate of change in NS gene. *Science* 232: 980–982.

Cox, N.J. & Subbarao, K. (2000) Global epidemiology of influenza: past and present, *Annu. Rev. Med*. 51: 407–421.

Ferguson, N.M., Galvani, A.P. & Bush, R.M. (2003). Ecological and immunological determinants of influenza evolution. *Nature* 422: 423–428.

Fitch, W.M., Leiter, J.M.E., Li, X. & Palese, P. (1991) Positive Darwinian evolution in human influenza A viruses, *Proc. Natl. Acad. Sci. USA* 88: 4270–4274.

Fitch, W.M., Bush, R.M., Bender, C.A. & Cox, N.J. (1997) Long term trends in the evolution of H(3) HA1 human influenza type A, *Proc. Natl. Acad. Sci. USA* 94: 7712–7718.

Gupta, S., Maiden, M.C.J, Feavers, I.M., Nee, S., May, R.M. and Anderson, R.M. (1996) The maintenance of strain structure in populations of recombining infectious agents. *Nat. Med*. 2: 437–442.

Hay, A., Gregory, V., Douglas A. & Lin, Y. (2001) The evolution of human influenza viruses. *Phil. Trans. R. Soc. Lond. B* 356: 1861–1870.

Koelle, K., Cobey, S., Grenfell, B. & Pascual, M. (2006). Epochal evolution shapes the phylodynamics of interpandemic influenza A(H3N2) in humans. *Science* 314: 1898–1903.

Minayev, P. & Ferguson, N. (2009) Improving the realism of deterministic multi-strain models: implications for modelling influenza A. *Interface* 6: 509–518

Rambaut, A., Pybus, O. G., Nelson, M. I., Viboud, C., Taubenberger, J. K. & Holmes, E. C. (2008). The genomic and epidemiological dynamics of human influenza A virus. *Nature* 453: 615-619

Recker, M., Pybus, O.G., Nee, S. & Gupta, S. (2007) The generation of influenza outbreaks by a network of host immune responses against a limited set of antigenic types. *Proc. Natl Acad. Sci. USA* 104: 7711-7716

Omori, R., Adams, B. & Sasaki, A. (2010) Coexistence conditions for strains of influenza with immune cross-reaction. *J. Theor. Biol*. 262: 48-57

Sasaki, A. & Haraguchi, Y. (2000) Antigenic drift of viruses within a host: A finite site model with demographic stochasticity. *Journal of Molecular Evolution* 51: 245-255

Supporting information 1.

Supporting figures referred in the main body. See legends for the explanation.

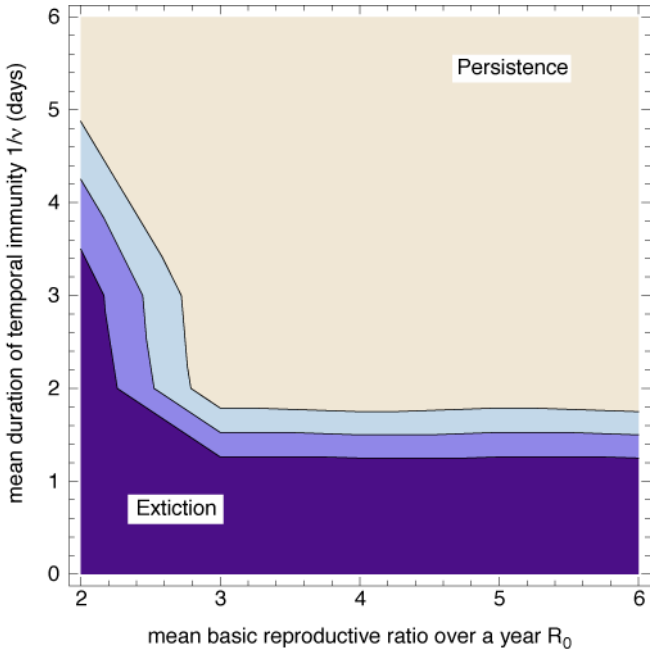

Figure S1: Persistence condition of virus in the IBM model when there is co-infection and general temporal immunity. We counted the frequency of simulation runs in which the lineage of virus survived over 70 years (over a generation time of host) in 20 simulation runs of individual based model. In the region marked as "Persistence", virus survived for over 70 years in all 20 simulation runs; whereas, in the region marked as "Extinction", virus went extinct within 70 years in all 20 simulation runs. The parameters except $\bar{R}_0$ and $1/\nu$ were set as $\alpha = 0.2$, $a = 0.6$, u = 1/50 and m = 0.001.

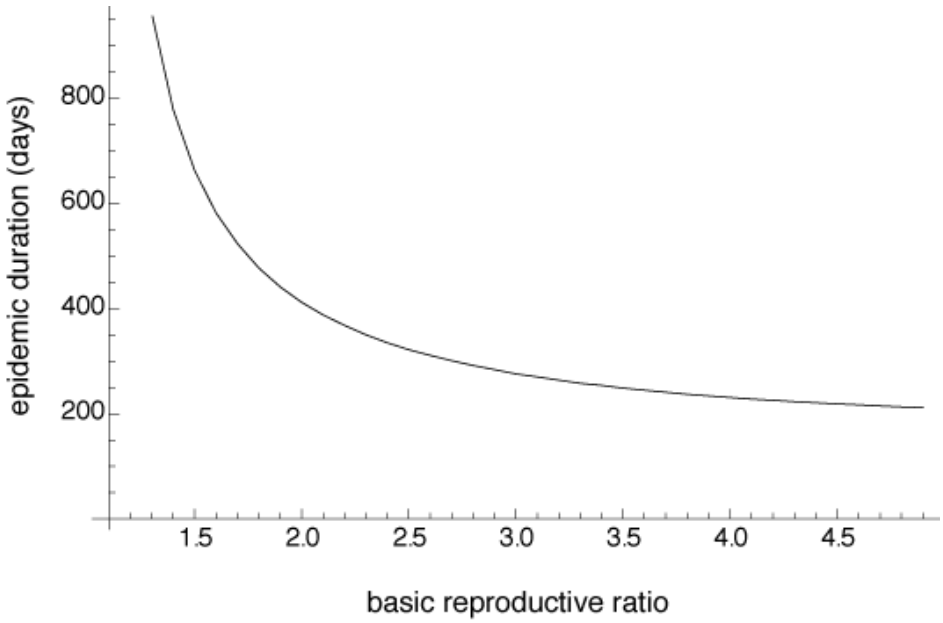

Figure S2: The dependence of epidemic duration on basic reproductive ratio in a single strain SIR model. Time course change of the frequencies of *S*, *I* and *R* in a single strain SIR model is $S' = -\beta SI, I' = \beta SI - \gamma I$, and $R' = \gamma I$. Mean duration of infectiousness is constant, $1/\gamma = 14$ (days), and the basic reproductive ratio β/γ is changed by changing β. Initial condition is $I(0) = 0.000001$, $S(0) = 1 - I(0)$, and $R(0) = 0$. The epidemic duration is defined as the duration from the beginning of simulation to the time when *I* will become smaller than the initial value of *I*, *I*(0).

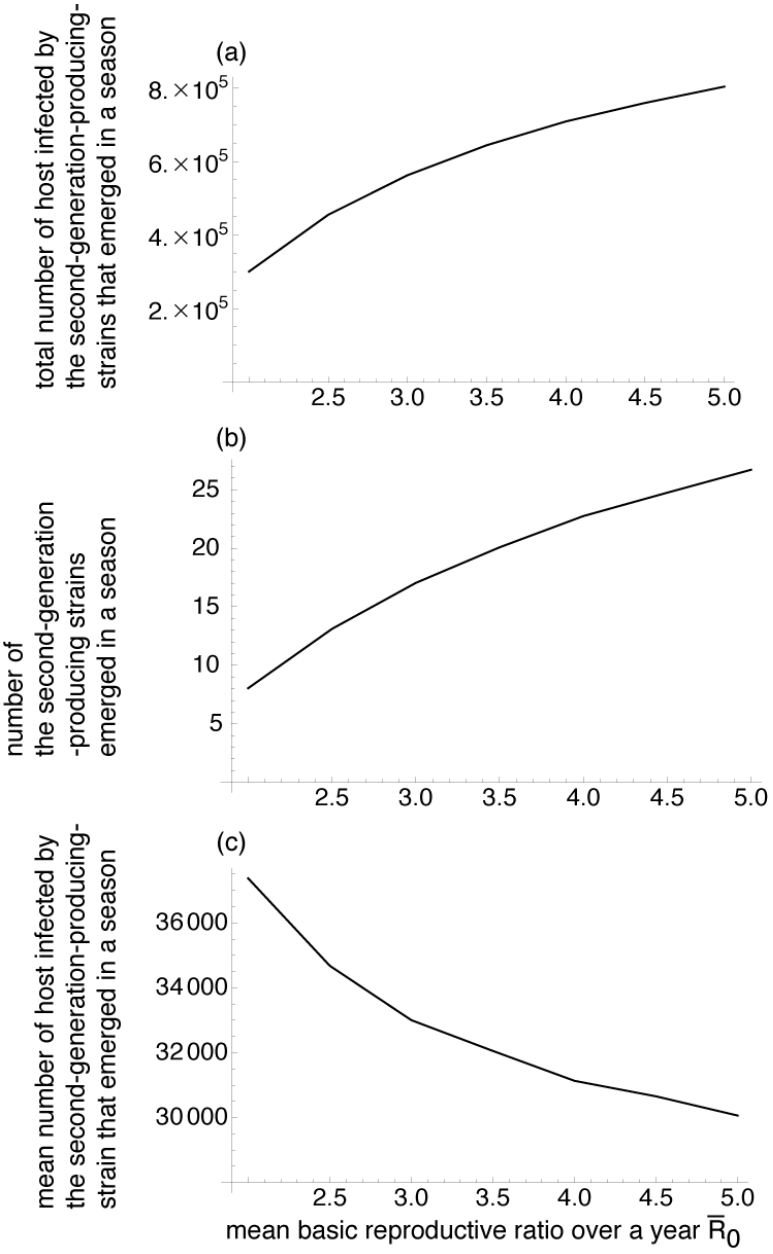

Figure S3: The relationship between $\overline{R}_0$ and (a) the total number of hosts infected with the second-generation producing strains that emerged in a season (b) the number of second-generation producing strains emerged in a season (c) the mean final epidemic size of each of second-generation producing strain, i.e. the mean number of hosts infected by each of second-generation producing strain. (a), (b) and (c) are generated from a 1000-year simulation in the IBM model. The parameters except $\overline{R}_0$ were set as $\alpha = 0.2$, $1/\nu = 7/365$ (7 days), $a = 0.6$, u = 1/50 and μ = 0.001.

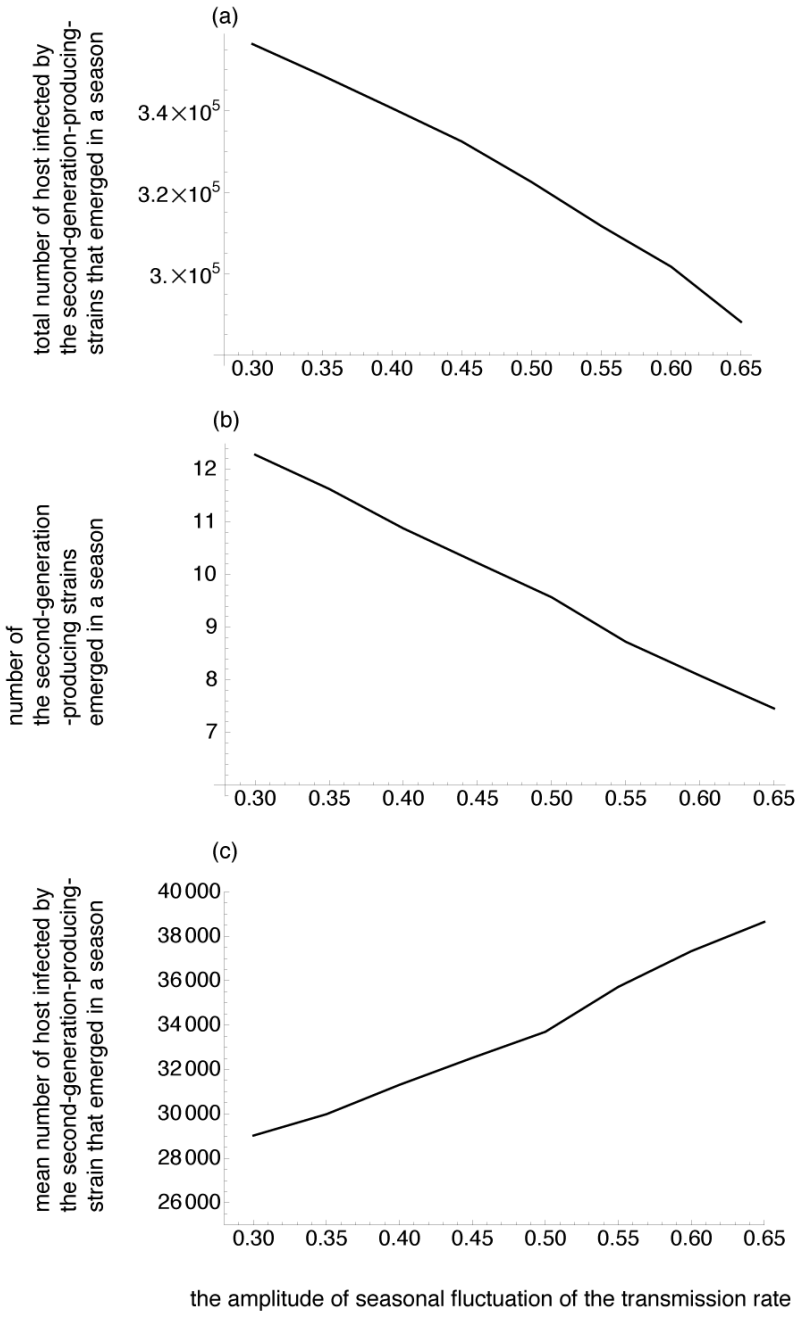

Figure S4: The relationship between the amplitude, a, of seasonal fluctuation of the transmission rate and (a) the total number of hosts infected with the second-generation producing strains that emerged in a season (b) the number of the second-generation producing strains emerged in a season (c) the mean final epidemic size of each of second-generation producing strains. (a), (b) and (c) are generated from a 1000-year simulation in the IBM model that the parameters except *a* were set as $\bar{R}_0 = 2$, $\alpha = 0.2$, $1/\nu = 7/365$ (7 days), u = 1/50 and μ = 0.001.

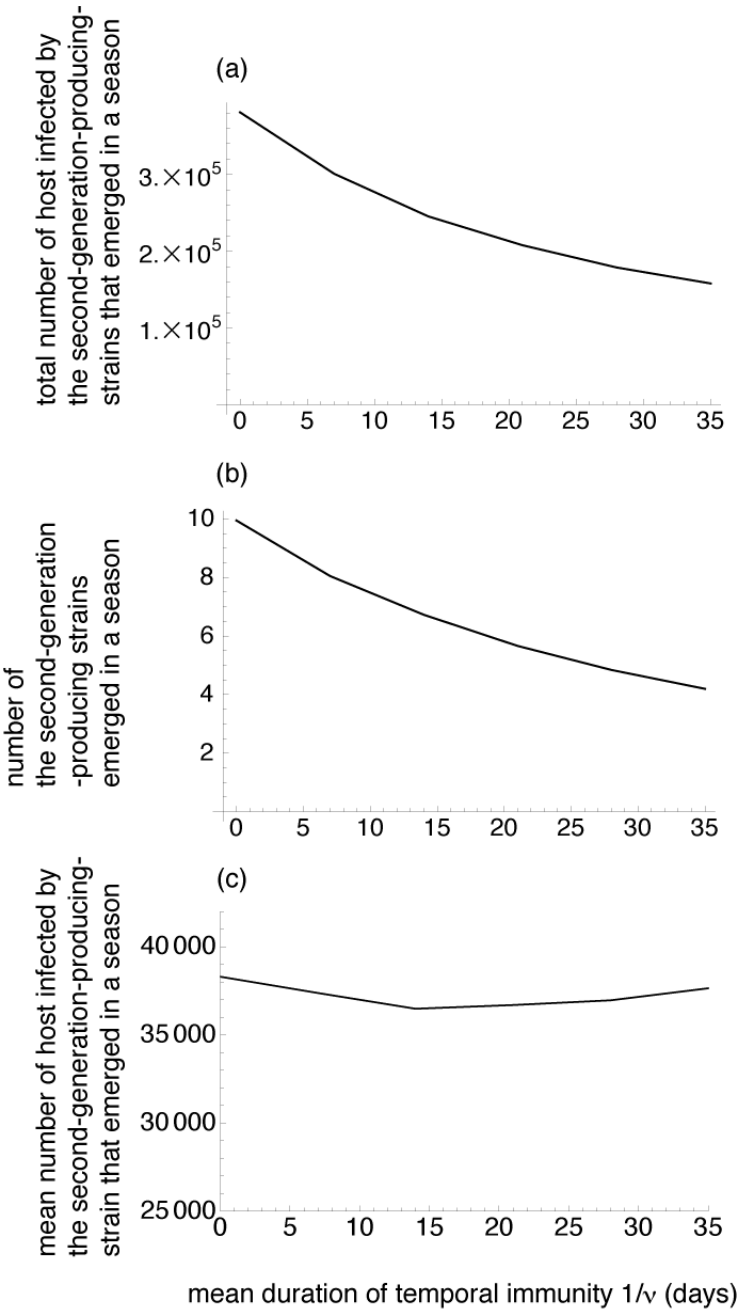

Figure S5: The relationship between mean duration of temporal immunity $1/\nu$ and (a) the total number of infected hosts with the second-generation producing strains that emerged in a season (b) the number of the second-generation producing strains that emerged in a season(c) the mean number of the hosts infected by each of second-generation producing strain that emerged in a season. (a), (b) and (c) are generated from a 1000 year IBM simulation that the parameters except $1/\nu$ were set as $\bar{R}_0 = 2$, $\alpha = 0.2$, $a = 0.6$, u = 1/50 and μ = 0.001.

Supporting information 2.

The demoted synchronization of epidemical peak timing with a larger basic reproductive ratio

For the analysis of the relationship between synchronization of epidemic peaks and basic reproductive ratio, we used a standard SIR model with seasonal fluctuation of transmission rate,

$$\begin{aligned} S' &= -\beta SI, \\ I' &= \beta SI - \gamma I, \\ R' &= \gamma I, \end{aligned} \qquad \text{(S1)}$$

where $S+I+R=1$ and $\beta(t)=\beta_0(1+a\cos(2\pi t))$. See Figure S6 legends for the parameter values and initial condition. Using this model, we analyzed the relationship between the emergence time *in a year* (i.e. introduction time of a strain into the host population) and epidemic peak timing *in a year*. If $\bar{R}_0$ is small, the epidemic peak times *in a year* are limited in a narrow range in a year when the emergence times are varied over a year; whereas, if $\bar{R}_0$ is large, the epidemic peak times varied over a wider range *in a year* (Figure S6a-c). This implies that a smaller $\bar{R}_0$ promotes synchronization of epidemic peak timing *in a year* among co-circulating strains that emerged at different emergence times.

"Mean-field" single strain model

To understand what makes the carry-over of epidemic peak time, we analyzed the key behavior of the IBM model (equation 16-19 in the main text) by constructing a simple deterministic model described below. In IBM model, the relative infectivity reduction by cross-immunity in the force of infection of a particular strain is determined by the mean susceptibility to this strain of host population (equation 17 and 19 in the main text). In this model, for the sake of simplicity, we assumed that the susceptibility to a particular strain is constant during the epidemic of this strain, and equals to the mean value observed in IBM simulations averaged over all emerged strains. Therefore the force of infection to strain A (equation 2 in main text) is rewritten by

$$\Lambda_A = \beta \bar{Q} i_A, \qquad \text{(S2)}$$

where i_A denotes the frequency of hosts infect with strain A, $\bar{Q}$ denotes the mean susceptibility and $\beta=\beta_0(1+a\cos(2\pi t))$.

Under these approximations, we now consider the epidemic dynamics of a

strain “in the mean field”, in which the influence of the other cocirculating strains is embedded in the mean host susceptibility. Suppose that co-infection is possible, but there is no general temporal immunity. The dynamics for the population of each immunity status to stain A, the hosts that are susceptible to strain A (s_A), the hosts that are currently infected and infectious with strain A (i_A), and the hosts that are immune to strain A (r_A), is described, with equation (S2), by

$$\begin{aligned} s_A' &= -\Lambda_A s_A, \\ i_A' &= \Lambda_A s_A - \gamma i_A, \\ r_A' &= \gamma i_A, \end{aligned} \tag{S3}$$

where $s_A + i_A + r_A = 1$ by definition. Here We used the mean value of the susceptibility to all strains in a 1000-year simulation of the IBM model with the same parameter values as the value of $\bar{Q}$; $\bar{Q} = 0.85$.

Next, we consider the case in which there *is* general temporal immunity but no co-infection. The time course of frequency of each immunity status is rewritten, with equation (S2), as follows

$$\begin{aligned} s_A' &= -\Lambda_A(s_A - \hat{i}(t) - \hat{w}(t)), \\ i_A' &= \Lambda_A(s_A - \hat{i}(t) - \hat{w}(t)) - \gamma i_A, \\ r_A' &= \gamma i_A \end{aligned} \tag{S4}$$

where $\hat{w}(t)$ denotes the frequency of hosts that have general temporal immunity, and $\hat{i}(t)$ denotes the frequency of hosts that are currently infected by some other strain. We used the mean frequency of hosts infected by any strain at each time in a year over 1000 years in the IBM model as $\hat{i}(t)$ and the mean frequency of hosts that have general temporal immunity at each time point in a year over 1000 years in the IBM model as $\hat{w}(t)$. For the calculation of $\hat{i}(t)$ and $\hat{w}(t)$ in the IBM model, the parameters were set as $\bar{R}_0 = 2$, $\alpha = 0.2$, $1/\nu = 7/365$ (7 days), $u = 1/50$ and $\mu = 0.001$.

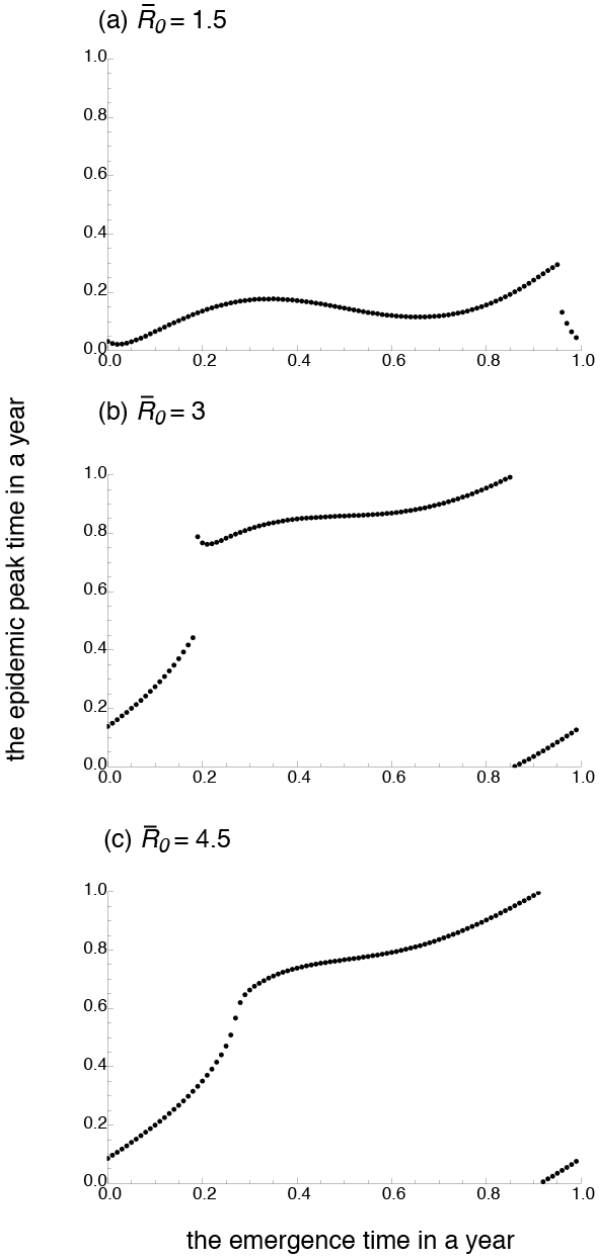

Figure S6: Relationship between the emergence time in a year and the epidemic peak time in a year. Points show the emergence time in a year (horizontal axis) and the epidemic peak time in a year (vertical axis). The emergence time in a year is varied from 0 to 0.99 year and with 0.01 year interval. The initial condition is that there are a few hosts infected ($I(0) = 0.000001$) and the other hosts are susceptible ($S(0) = 1 - I(0)$, $R(0) = 0$). The mean basic reproductive ratio $\bar{R}_0 = \bar{\beta} / \gamma$ was adjusted by changing $\bar{\beta}$. The parameters were set as $a = 0.6$ and $1/\gamma = 14/365$ (14 days).

Figure legends

Figure10. The distribution of the emergence times of new strains observed in a 1000-year simulation run of the IBM model. a: The solid line indicates the distribution of the timing in each year of the number of epitope changing strains emerged by mutation with the moving averaged of 1/10 year window. The dashed line indicates the seasonally varying transmission rate. b-d: The conditional distributions for the timing of the emergence of strains that succeeded to produce the second generation (b), the third generation (c), and the forth generation (d). The parameters were set as $\bar{R}_0 = 2$, $\alpha = 0.2$, $1/\nu = 7/365$ (7 days), $a = 0.6$, $1/u = 50$ (years), and $\mu = 0.001$ (per infection).

Figure 11. The peak emergence times of all the new strains, and the subset of successful (the second-, the third-, and the forth-generation producing) strains as functions of epidemiological parameters. In each panel, black line shows the peak emergence time (relative to a year – see the scale of the horizontal axis of Figure10) of all the new strains (antigenicity mutants); blue, red, green lines, that of the second-, the third-, and the forth-generation producing strains. The epidemiological parameters varied along the horizontal axis of each panel are: (a) the mean basic reproductive ratio averaged over a year, $\bar{R}_0 = \beta_0/(u+\gamma)$, (b) the infectivity reduction α by the cross immunity mounted by a single-step distant strain, (c) the mean duration of temporal immunity, $1/\nu$, and (d) the amplitude of seasonal fluctuation of transmission rate, a. Each point represents the mean value of 10,000 times boot-strap resampling of the simulation results over 1000 years, and the error bars denote their standard deviations. Apart from the parameter values varied in the horizontal axis, the other parameters were set to $\bar{R}_0 = 2$, $\alpha = 0.2$, $1/\nu = 7/365$ (7 days), $a = 0.6$, u = 1/50 and μ = 0.001.

Figure 12. The cumulative distribution for the timing of infections of all the strains that emerged in a 1000-year simulation of the IBM model. The vertical axis denotes the cumulative distribution for the timing of infection, i.e., the number of hosts infected by a strain by time t, divided by the final epidemic size of that strain. (a) The distribution for varying mean basic reproductive rate over a year, $\bar{R}_0$, from 2 to 4, (b) that for varying infectivity reduction rate by cross-immunity, α, from 0.1 to 0.3, (c) that for varying mean duration of temporal immunity, $1/\nu$, from 2 to 36 days, and (d) that for

varying amplitude of seasonal fluctuation of transmission rate, a, from 0.3 to 0.6. The basic parameters were set as $\bar{R}_0 = 2$ (b-d), $\alpha = 0.2$ (a, c, d), $1/\nu = 7/365$ (7 days; a, b, d), $a = 0.6$ (a-c), $1/u = 50$ (years), and $\mu = 0.001$ (per infection).

Figure 13. The relationship between the time of the emergence of a strain in a year (horizontal axis) and the waiting time until the number of infected hosts attains its peak since it emerges (vertical axis, in units of year). Note that the transmission is maximum at $t = 0$ or $t = 1$, and is minimum at $t = 1/2$. The vertical axis greater than 1 indicates that the epidemic peak is carried over to the next year from the year of emergence. Red points indicate the median of the waiting time, observed in a 1000-year simulation of the IBM model, until a second-generation producing strain attains its peak epidemic size. Blue points are the result for "mean-field" single strain model described in Supporting Information 2 when there *is* co-infection but *no* general temporal immunity. Green points are the result for the same mean-field single strain model but now there *is* general temporal immunity but *no* co-infection. The parameters were $\bar{R}_0 = 2$, $\alpha = 0.2$, $1/\nu = 7/365$ (years, or 7 days), $a = 0.6$, $1/u = 50$ (years) and $\mu = 0.001$.

Figure 14. The epidemic duration of the second-generation-producing strain in a 1000-year simulation of the IBM model. Each line denotes mean values of the epidemic duration of the second-generation-producing strains and error bar is standard deviation. Apart from the parameter values varied in the horizontal axis, the other parameters were set to $\bar{R}_0 = 2$, $\alpha = 0.2$, $1/\nu = 7/365$ (7 days), $a = 0.6$, u = 1/50 and μ = 0.001.

Figure
Figure 10.

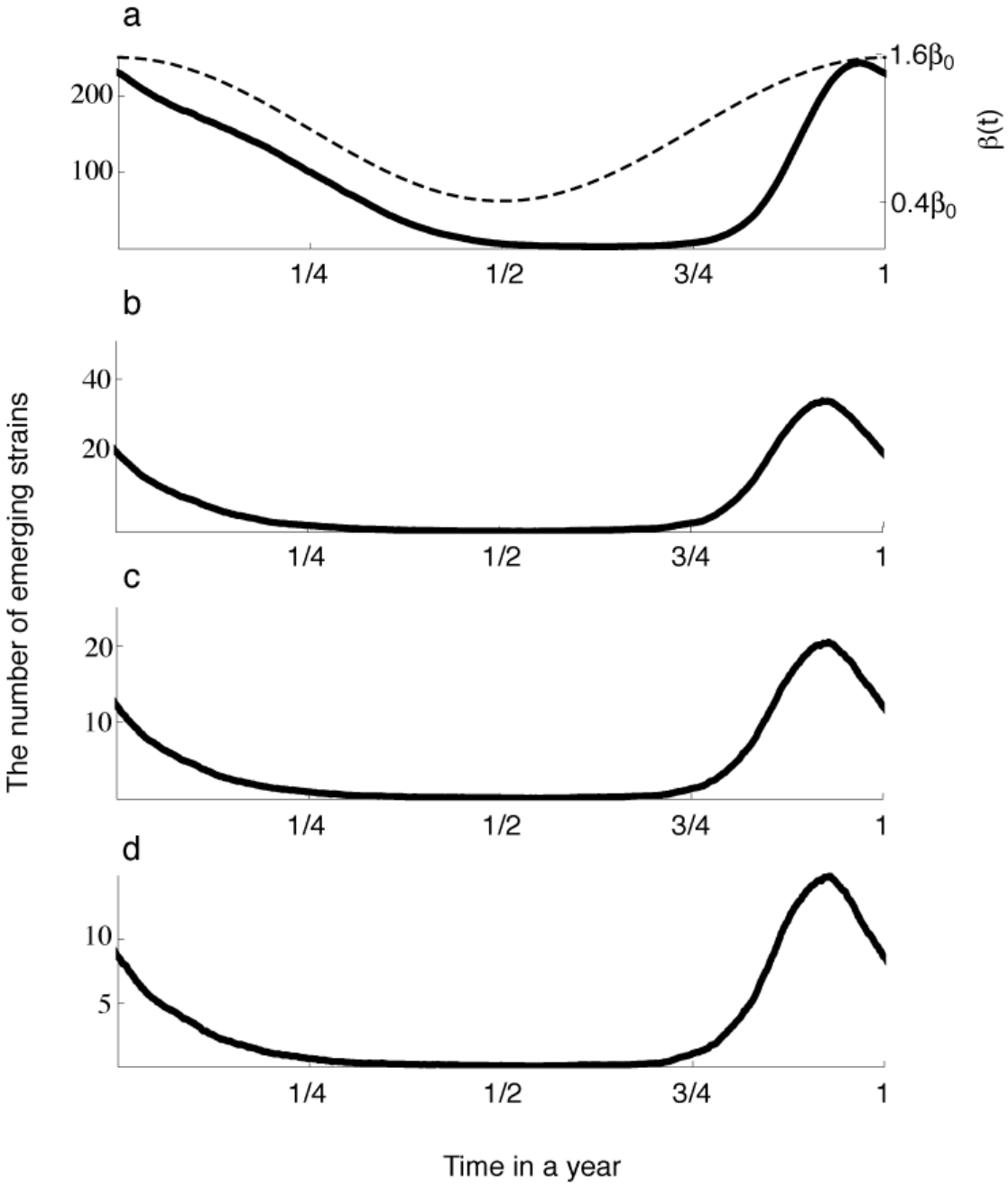

Figure 11.

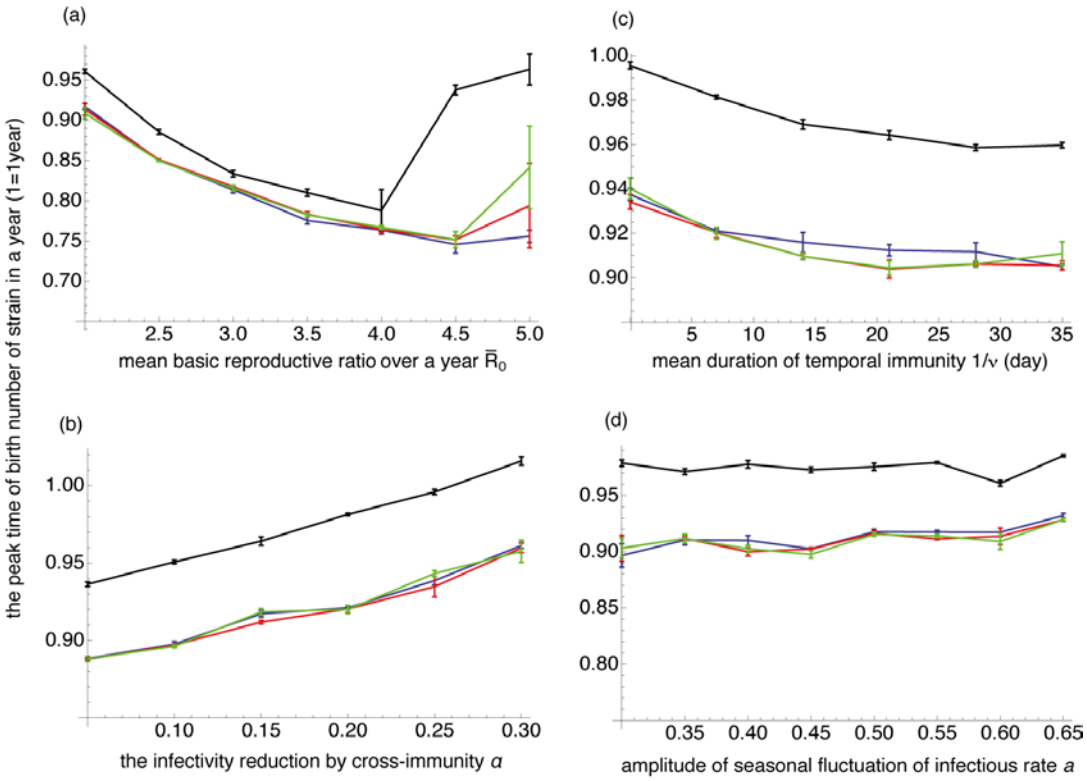
(a)
(b)
(c)
(d)
the peak time of birth number of strain in a year (1=1year)
mean basic reproductive ratio over a year $\bar{R}_0$
the infectivity reduction by cross-immunity α
mean duration of temporal immunity $1/\nu$ (day)
amplitude of seasonal fluctuation of infectious rate a

Figure 12.

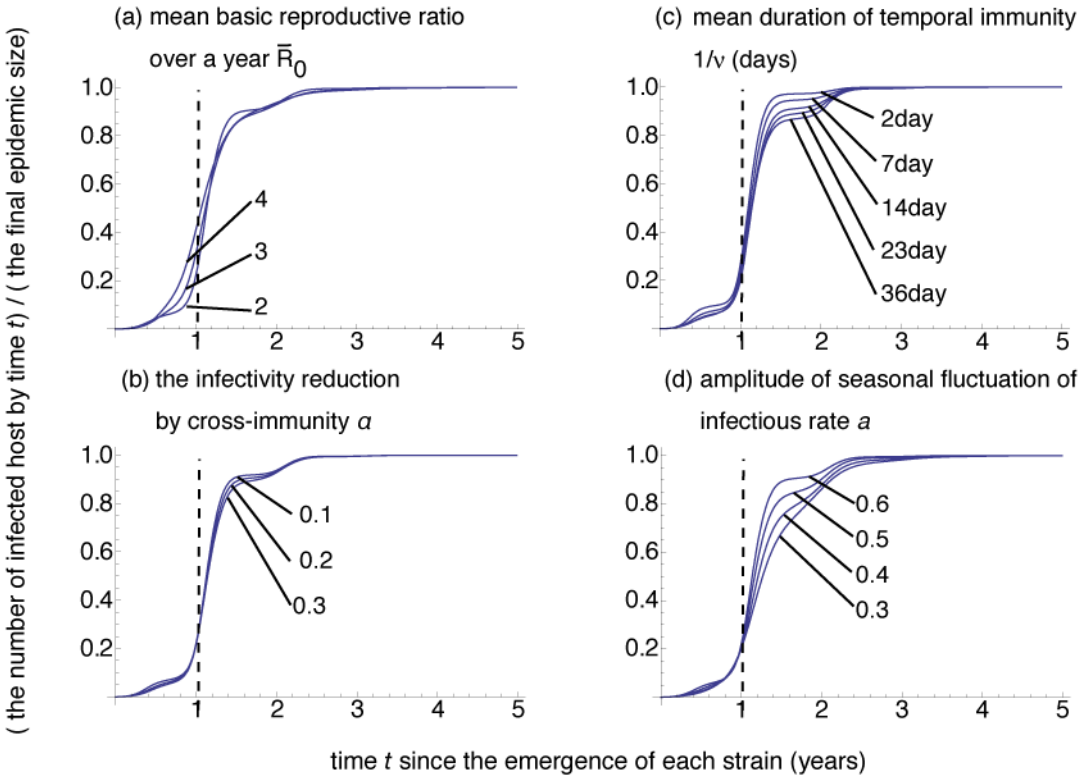
(a) mean basic reproductive ratio
over a year $\bar{R}_0$
(c) mean duration of temporal immunity
1/ν (days)
2day
7day
14day
23day
36day
4
3
2
(b) the infectivity reduction
by cross-immunity *a*
(d) amplitude of seasonal fluctuation of
infectious rate *a*
0.1
0.2
0.3
0.6
0.5
0.4
0.3
(the number of infected host by time *t*) / (the final epidemic size)
time *t* since the emergence of each strain (years)

Figure 13.

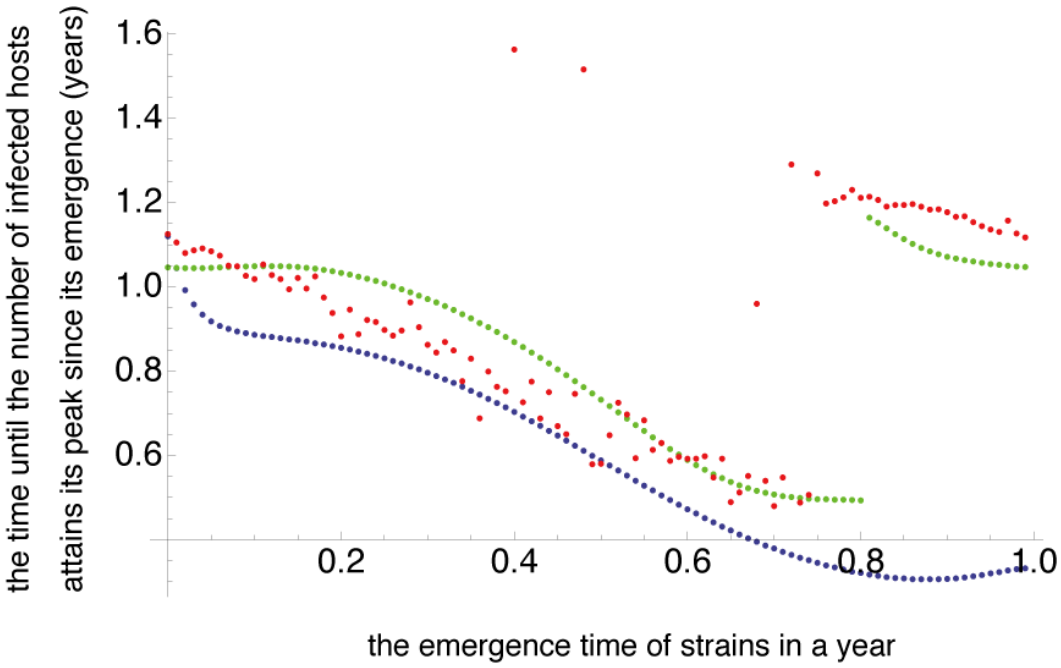
the time until the number of infected hosts attains its peak since its emergence (years)
1.6
1.4
1.2
1.0
0.8
0.6
0.2
0.4
0.6
0.8
1.0
the emergence time of strains in a year

Figure 14.

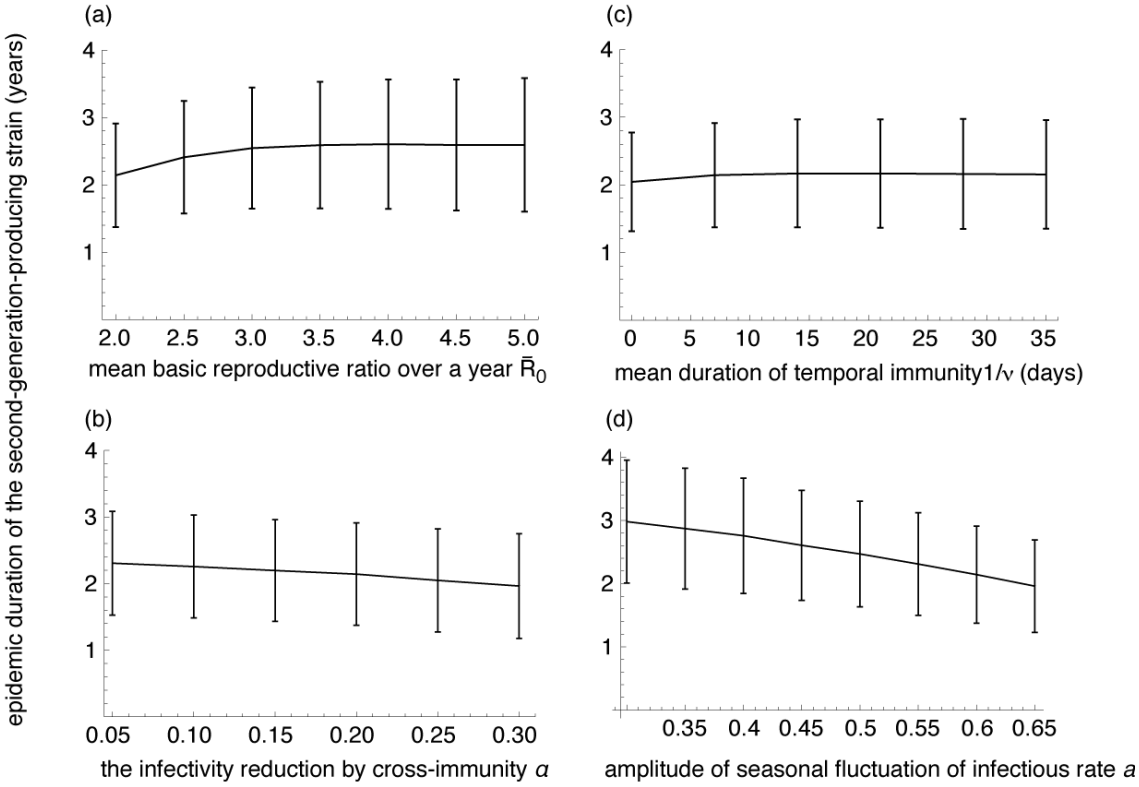
(a)
(c)
(b)
(d)
epidemic duration of the second-generation-producing strain (years)
mean basic reproductive ratio over a year $\bar{R}_0$
mean duration of temporal immunity $1/\nu$ (days)
the infectivity reduction by cross-immunity α
amplitude of seasonal fluctuation of infectious rate a

Chapter 3

Disrupting seasonality to control disease outbreaks: The case of koi herpes virus

The study of this chapter, done in collaboration with Dr. Ben Adams, was published in Journal of Theoretical Biology (271, pp159-165) in 2011.

Introduction

The dynamics of many infectious diseases are governed by seasonally varying factors. As reviewed in Altizer et al. 2006, for example, aggregation patterns associated with the school year drive the transmission of measles. Seasonal variation in rainfall drives the transmission of cholera. The incidence of vector-borne disease such as malaria, dengue and West Nile virus is influenced by the effects of temperature and rainfall on mosquito population sizes and viral incubation rates. Many authors have used mathematical models to study the role of natural seasonality in epidemiological dynamics. They have shown that the effects of seasonally varying epidemic drivers may go far beyond simply correlated patterns of incidence (e.g. London and Yorke 1973; Dietz 1976; Hethcote and Yorke 1980; Schwartz and Smith 1983; Aron and Schwartz 1984; Schwartz 1985; Keeling et al. 2001; Greenman et al, 2004; Adams and Boots, 2007). In some cases, it has also been shown that it may be possible to moderate or control disease outbreaks by disrupting the normal seasonal pattern of transmission, for instance by closing schools. Here we take koi herpesvirus (KHV) as a case study. We examine how seasonal variation in water temperature affects KHV epidemiology, and consider how outbreaks may be controlled by managing the water temperature.

Common carp (*Cyprinus carpio*) is cultivated for food in many countries. In 2002 it accounted for 14% of global freshwater aquaculture production (Peteri, 2005). The koi subspecies is also of economic importance as an ornamental fish. Koi herpesvirus is in the family *herpesviridae* (Waltzek et al. 2005). It infects common and koi carp and is highly virulent (Perelberg et al. 2003; Ronen et al. 2003; Pikarsky et al. 2004). The first report of KHV was in 1998 in Israel. Since then it has also been reported in the US and many European and Asian countries (Perelberg et al. 2003; Walster, 1999; Hedrick et al. 2000; Miyakazi et al. 2000; Oh et al. 2001; Taylor et al. 2010). KHV represents a series economic threat to the freshwater aquaculture industry. The epidemiology of KHV shows marked seasonality related to water temperature. Outbreaks are generally observed in spring or autumn and do not occur when water temperatures are high in summer, or low in winter (Yuasa et al. 2008; Gilad et al. 2003). On the basis of this temperature dependence, it has been proposed that KHV outbreaks in isolated aquaculture environments could be controlled by increasing the water temperature beyond the limit for viral growth. However, it has been reported that carp treated in this way may become symptomatic again after the treatment is stopped and it

has been suggested that this control strategy may suppress the epidemic, but not stop it completely (Iida and Sano, 2005).

In this article we introduce and analyse a mathematical model for KHV epidemiology that, based on published experimental data, is driven by seasonally varying delays between infection and infectiousness, infectiousness and mortality. The model is developed from a delay differential equation framework with variable delay originally introduced to study stage-structured insect population dynamics (Nisbet and Gurney, 1983). After introducing the model we consider the dynamics of outbreaks starting at different times of year under natural seasonality. We then consider the impacts, and risks, of attempting to control outbreaks by water temperature management.

Model

We developed a mathematical model for the epidemiology of KHV based on the published observations of experimental infections. Yuasa et al. (2008) tested infectiousness by infecting groups of fish and then exposing naive fish to them at fixed time intervals. Their observations indicate that a minimum incubation period is required between infection and infectiousness. The rate of progression through this 'exposed' state depended on temperature in a non-monotonic way, with a maximum rate, equating to a duration of approximately 1 day, at 23°C (Fig. S7a). In separate experiments, Yusua et al. (2008) assessed KHV mortality by monitoring groups of fish following exposure to the virus. They found that no deaths at all occurred for several days after infection but high mortality followed. The duration of this delay also depended on temperature with the shortest periods, of approximately four days, occurring at 23°C and 28°C (Fig. S7b). Similar results were reported by Gilad et al. (2003). Combined with the data on the time between infection and infectivity, these observations suggest that, after the incubating state, there is a second temperature dependent state in the progression of KHV when the fish is infectious but viremia is not sufficient to cause death. After the delay of the exposed and infectious states, the experimental observations indicated that the fish entered an 'ailing' state where mortality was rapid and largely independent of temperature (Fig. S7c). A proportion of the cohort, however, did not die, suggesting that they had recovered from the infection and gained immunity.

On the basis of these observations, we classify the model population into five states with respect to KHV infection: susceptible *S*, exposed *E*, infectious *I*, ailing *A* and recovered *R*. States *I* and *A* are infectious and new infections occur at rate $\beta S(I + A)$. We assume that a cohort of fish infected simultaneously all become infectious after exactly the same waiting period in the *E* state, the duration of which τ_E depends only on water temperature T. In the same way, the duration of the infectious state (*I*) is modelled by a temperature dependent delay $\tau_I = \tau_I(T)$. We express the natural seasonality in water temperature $T(t)$ by a cosine function. St Hilaire et al. (2009) conducted experiments in which they observed a significant lag between exposure to KHV and detectable antibodies. We approximate this delay by assuming that fish in state *E* do not recover but fish in states *I* and *A* recover, and enter state *R*, at rate η. Fish in all states are subject to natural mortality at rate μ. Fish in state *A* are also subject to disease induced mortality at rate ξ.

These considerations lead to a system of differential equations with two temperature dependent delays $\tau_E(T(t)), \tau_I(T(t))$. As detailed in the Supplementary Information, to find expressions for these delays we define $\gamma(T(t))$ to be a scaled form of a notional rate of increase of viremia following infection, estimating the temperature dependence by fitting a Weibull function to the data of Yuasa et al. (2008) (see Figs. S7a,b). Then, following the derivation set out in detail for stage-structured insect populations by Nisbet and Gurney (1983) and Nisbet (1997), and also given in the Supplementary Information, we arrive at the delay differential equation model

$$
\begin{aligned}
&\frac{dS}{dt} = -\beta S(t)[I(t)+A(t)] - \mu S(t),\\
&\frac{dE}{dt} = \beta S(t)[I(t)+A(t)] - \beta S(t_E^-)[I(t_E^-)+A(t_E^-)]\frac{\gamma(t)}{\gamma(t_E^-)}P_E(t) - \mu E(t),\\
&\frac{dI}{dt} = \beta S(t_E^-)[I(t_E^-)+A(t_E^-)]\frac{\gamma(t)}{\gamma(t_E^-)}P_E(t)\\
&\qquad - \beta S(t_{EI}^-)[I(t_{EI}^-)+A(t_{EI}^-)]\frac{\gamma(t)}{\gamma(t_{EI}^-)}P_E(t_I^-)P_I(t) - (\mu+\eta)I(t),\\
&\frac{dA}{dt} = \beta S(t_{EI}^-)[I(t_{EI}^-)+A(t_{EI}^-)]\frac{\gamma(t)}{\gamma(t_{EI}^-)}P_E(t_I^-)P_I(t) - (\mu+\eta+\xi)A(t),\\
&\frac{dR}{dt} = \eta(I(t)+A(t)) - \mu R(t),\\
&\frac{d\tau_E}{dt} = 1 - \frac{\gamma(t)}{\gamma(t-\tau_E(t))}, \quad \frac{d\tau_I}{dt} = 1 - \frac{\gamma(t)}{\gamma(t-\tau_I(t))}.
\end{aligned}
\tag{20}
$$

We assume closed population of host, birth/death of host does not occur and number of initial infected host is small enough. The symbol denotes each state of host (*S*, *E*, *I*, *A* and *R*) is proportion to initial value of whole hosts. Here $P_E(t) = \exp(-\mu\tau_E(t))$ is the proportion of the original cohort that survived the incubation period to mature from state *E* at time *t*, $P_I(t) = \exp(-(\mu+\eta)\tau_I(t))$ is similarly defined for state *I*, and

$$
\begin{aligned}
t_E^- &= t - \tau_E(t)\\
t_I^- &= t - \tau_I(t)\\
t_{EI}^- &= t - \tau_E(t-\tau_I(t)) - \tau_I(t)
\end{aligned}
\tag{21}
$$

All parameter values are given in Table 1. The system was solved numerically using the solv95 package in C and initial conditions $S(t) = 1, E(t) = A(t) = R(t) = 0$ for $t < t_0$,

$I(t_0) = 0.001, S(t_0) = 0.999, E(t_0) = A(t_0) = R(t_0) = 0,\ \tau_E(t_0)$ such that $\int_{t=t_0-\tau_E(t_0)}^{t_0} \gamma(t)dt = 1,$

$\tau_I(t_0)$ such that $\int_{t=t_0-\tau_I(t_0)}^{t_0} \frac{\gamma(t)}{4}dt = 1.$

Results

We analysed the model dynamics to investigate how natural seasonal variation in water temperature is related to the extent of KHV epidemics, and how epidemics may be moderated by artificially controlling water temperature. First, we

consider some of the fundamental implications of the seasonal variation in the delay between infection and infectiousness, infectiousness and mortality.

Basic epidemiology without treatment

The delay term $\tau_E(t)$ is defined such that fish that entered the exposed state (*E*) at time $t - \tau_E(t)$ move to the infectious state (*I*) at time *t*. The term $\tau_I(t)$ is similarly defined for the delay between entering the infectious state (*I*) and moving to the ailing state (*A*). So, $\tau_E(t)$ and $\tau_I(t)$ are the delay times looking backward. We also define the delay time looking forward, $\hat{\tau}_E(t)$, such that fish entering state *E* at time *t* will move to state *I* at time $t + \hat{\tau}_E(t)$. The forward delay $\hat{\tau}_I(t)$ is similarly defined for the transition from state *I* to state *A*. Seasonal variation in temperature results in seasonal variation in $\hat{\tau}_E(t)$ and $\hat{\tau}_I(t)$ (Fig. 15a). However, the skewed relationship between temperature and the rate at which infection progresses means that the delay terms do not track the temperature fluctuations in a straightforward manner. The delays suddenly increase in autumn, around the midpoint of the seasonal decline in water temperature, and then decrease monotonically until spring. This pattern is indicative of the decreasing waiting time until the temperature becomes permissive for the development of KHV. The delays remain fairly constant between spring and autumn because disease progression is rapid for most of this period and the duration of the non-permissive temperatures in mid-summer is short.

The basic reproductive number R_0 is generally defined such that the transition between long-term dynamics characterized by disease free and endemic states occurs at the threshold $R_0 = 1$. In non-seasonal environments this definition of R_0 is usually consistent with the interpretation of R_0 as the expected number of secondary infections caused by a single infected individual in an otherwise susceptible population. In seasonal environments, this expected number of secondary infections depends on the time at which the infected individual was introduced. Therefore, in order to preserve the threshold definition of R_0, the number of secondary infections resulting from a single infectious individual introduced to a naive population at time *t* is termed the (time-dependent) effective reproductive number $R_e(t)$ (Grassly and Fraser, 2006; Nishiura and Chowell, 2009). Here we are interested in disease outbreaks, rather than endemic circulation, and so focus on the effective reproductive number. In order to

construct $R_e(t)$, let $J(\phi)$ be the density of individuals in states I and A combined at time ϕ. Then

$$\frac{dJ}{d\phi} = \begin{cases} \frac{dI}{d\phi} = -(\mu+\eta)J & if \quad \phi - t \le \hat{\tau}_I(t) \\ \frac{dA}{d\phi} = -(\mu+\eta+\xi)J & if \quad \phi - t > \hat{\tau}_I(t) \end{cases} \tag{22}$$

we focus on expected number of secondary infection by individuals who become state I at just time t, therefore, $J(t) = 1$ as a initial condition of J. Solving

$$J(\phi) = \begin{cases} \exp(-(\mu+\eta)(\phi - t)) & if \quad \phi - t \le \hat{\tau}_I(t) \\ \exp(-(\mu+\eta)\tau_I(t))\exp(-(\mu+\eta+\xi)(\phi - t - \tau_I(t))) & if \quad \phi - t > \hat{\tau}_I(t) \end{cases} \tag{23}$$

Then, noting that if secondary infection occurs at time ϕ, the probability that the newly infected individual will survive until progressing to state I is $P_E(\phi) = \exp(-\mu\hat{\tau}_E(\phi))$, the effective reproductive number is

$$\begin{aligned} R_e(t) = \beta[& \int_{\phi=t}^{t+\tau_I(t)} \exp(-(\mu+\eta)(\phi - t))\exp(-\mu\hat{\tau}_E(\phi))d\phi + \\ & \int_{\phi=t+\tau_I(t)}^{\infty} \exp(-(\mu+\eta)\hat{\tau}_I(t))\exp(-(\mu+\eta+\xi)(\phi - t - \hat{\tau}_I(t)))\exp(-\mu\hat{\tau}_E(\phi))d\phi] \end{aligned} \tag{24}$$

The time dependence of the effective reproductive number $R_e(t)$ is shown in Fig. 1b. The effective reproductive number is highest during winter, and lowest during early and late summer. $R_e(t)$ is high when the delay $\hat{\tau}_I$ is long, for instance at the beginning of winter, because infectious fish live longer as disease induced mortality only occurs in the A state. $R_e(t)$ is small when the delays are short because infectious fish rapidly move to the ailing state and die.

Farmed carp are harvested after around two years. We now assume that a cohort contaminated with a single infectious individual is established at time t_0 and consider the state of the population when it is harvested at time t_0 + 730 (days). An equivalent interpretation is that an established cohort is first infected at time t_0 and then maintained for a further two years. Fig. 1c shows the total proportion of the cohort that dies due to KHV, and the total proportion of the cohort that becomes immune. Immunity is negatively correlated with mortality. The greatest total mortality occurs if the cohort

is established when $\hat{\tau}_E$ and $\hat{\tau}_I$ are short, in early and late summer. Large epidemics occur even if the infection is introduced in winter, when the delays $\hat{\tau}_E$ and $\hat{\tau}_I$ are long because the secondary infected fish just remain in the latent state until spring when τ_E and τ_I become shorter. Strikingly, the smallest outbreaks occur when the infected cohort is established at the end of autumn. At this time infected (*E*) fish quickly become infectious (*I*) because $\hat{\tau}_E$ is short (Fig 1a). However, $\hat{\tau}_I$ is long and, as Fig. 16 shows, most of these fish in the *I* state recover to the *R* state rather than progressing to the ailing state (*A*) and dying. In general, however, the seasonal changes in the delays mean that, if an infected cohort is established when $\hat{\tau}_E$ and $\hat{\tau}_I$ are long, the epidemic is simply postponed. Consequently mortality is seasonal, and concentrated in summer, regardless of when the initial infection occurs (Fig. S8).

Outbreak control using a single period of treatment

We now consider the impact of managing water temperature in order to control a KHV epidemic. We assume that, as soon as a specified outbreak measure exceeds a given threshold, the entire aquaculture environment is maintained for a fixed length of time at a constant temperature that is non-permissive for KHV development ($T = 33°C$). We consider outbreak measures defined by the instantaneous frequency of infectious and ailing fish $(I + A)^*$ and the cumulative frequency of KHV related mortality D^*. Initially we assume that treatment is only provided once, even if the outbreak thresholds are subsequently exceeded again. Carp aquaculture usually begins with new cohorts in spring, so we assume that an infected cohort is established at t_0 = 90.

We first consider the outbreak measure defined by the frequency of infectious fish. Fig. 17a shows the relationship between the total proportion of the cohort that dies due to KHV within the two years of aquaculture, the duration of the treatment by temperature control, and the infection threshold at which the treatment is started. In terms of the timing of treatment, it is most effective if it is started when the frequency of infectious fish is just before its maximum (Fig. 17a, $(I + A)^* \approx 0.64$). However, if the treatment is started slightly after this critical frequency, which will be extremely difficult to pinpoint during the course of an outbreak, it has almost no impact at all. The

high water temperature extends the waiting times in the *E* and *I* states. The extended time in the infectious state means that that the majority of infectious fish recover rather than die. The treatment is most effective when the proportion of the cohort that is infectious, and may recover, is large but the proportion that is latently infected, and may become infectious when treatment stops, is small. Starting the treatment too soon reduces its effectiveness because it only postpones the epidemic. Worse, it can increase total mortality relative to no treatment, as indicated by the white areas in Fig. 17a. In the early stages of the outbreak, the majority of infected fish are in still in the exposed state (*E*). Since exposed fish cannot gain immunity and recover, the high temperature simply causes these fish to remain in this state until the treatment is stopped. If the treatment period ends when temperatures allow rapid KHV progression, these fish restart an epidemic in which fish rapidly enter the ailing state and have only a brief opportunity to recover.

As regards the duration of treatment, mortality is lowest when temperature control is maintained for around 160 days. The difference between this low point and the mortality associated with shorter treatment durations is marked, particularly when the threshold infection frequency for the start of treatment is low. This sudden decrease occurs because of the time of year when the treatment ends. Previously we showed that infected cohorts established at the end of autumn have markedly lower mortality than cohorts established at any other time of year because the *E* state is brief but the *I* state is long, leading to extensive immunity. Similarly, treatment is particularly effective when the start time, which is determined by the infection frequency, and the duration combine such that the treatment ends when the forward delay in the *E* state is short, but the forward delay in the *I* state is long. Then, as shown in Fig. 18, the backward delay in the *E* state (τ_E, where a fish that moves from the *E* state to the *I* state at the current time was initially infected τ_E days previously), decreases sharply soon after the treatment ends but the backward delay in the *I* state τ_I continues to increase monotonically. Consequently, fish leave the *E* state and accumulate in the *I* state. As the seasonal temperature continues to fall, progression between all states slows and many of these fish recover before temperatures increase in spring.

We now consider the outbreak measure defined by the cumulative frequency of dead fish. Since it may be difficult to accurately identify infectious or ailing fish, particularly in large populations, this threshold may be easier to apply in practice. The

detection of mortality due to KHV means that there are fish in the ailing (*A*) state and the infection has already spread extensively through the population. Starting treatment earlier, i.e. at lower mortality thresholds, is increasingly effective at suppressing further mortality (Fig. 17b). It cannot lead to an increase in the total mortality relative to no treatment because the majority of fish are already in the *I* state, and there cannot be another major outbreak if temperatures become permissible again. Longer duration treatments generally reduce total mortality by allowing more fish to recover to the immune state. However, if the mortality threshold at which treatment is started is low ($D < 0.1$), the latent population is still sufficiently large that extending treatment beyond approximately 150 days can marginally reduce its effectiveness.

Outbreak control using several periods of treatment

A single period of treatment can effectively reduce the mortality associated with a KHV epidemic if it is initiated at the correct point in the outbreak, and maintained for a sufficiently long time. However, only continuing the treatment for long enough can render it ineffective. Starting the treatment too early be counterproductive. We now consider the impact of applying more than one treatment bout. As before, we assume that, as soon as the frequency of infectious and ailing fish exceeds a given threshold, the entire aquaculture environment is maintained for a fixed length of time at a constant temperature that is non-permissive for KHV development. It is then returned to the normal environmental temperature. However, if the outbreak threshold is exceeded again, another bout of temperature control is started, and maintained for the same duration as the first bout. We consider the impact of allowing up to two, or up to three, bouts of temperature control.

As Fig. 19a shows, two treatment bouts are generally very effective for controlling KHV outbreaks. The main exception is when the duration of each treatment bout is short and the outbreak threshold for the start of treatment is low. Then treatment can increase mortality relative to an outbreak that is not treated. If the outbreak threshold for beginning treatment is high, then only one treatment bout is used, even though this is less effective than using two bouts at a lower threshold (Fig. 19b). In this case, there is a resurgence of infections after the treatment is stopped, but it is not sufficient to trigger further treatment. Employing three treatment bouts, rather than two, leads to a small improvement in the effectiveness of short duration treatments, but has

little impact otherwise (Fig. S9).

Discussion

We have introduced a mathematical model for koi herpesvirus epidemiology characterized by temperature dependent periods in latent and infectious states before progression to an ailing state in which mortality is high. We have used this model to examine how seasonal fluctuations in water temperature drive the epidemiology of koi herpesvirus, and analysed how disrupting this seasonal pattern can be employed as an outbreak control strategy.

In our model the delay between infection and infectiousness is shorter than the delay between infectiousness and ailing at all temperatures, as observed in experiments (Yuasa et al. 2008). The water temperature fluctuates between 5℃ and 28℃ over the course of a year, as observed in lake Kasumigaura, Japan. We have shown that, under these conditions, disease progression is rapid in summer and slow in winter. But the morality associated with outbreaks that start in winter is only slightly lower than those that start in summer because fish remain in the latent class, rather than recovering, until spring. However, outbreaks that start during a brief interval at the end of autumn can result in low mortality and widespread immunity. At this time a phase shift in the delays associated with the latent and infectious states allows fish to progress from the latent to the infectious state, where recovery occurs throughout the winter, but prevents them from progressing to the high mortality ailing state. A major concern in aquaculture is the possibility of KHV contamination in a newly established cohort. Our analysis suggests that introducing new cohorts, or importing new fish into an existing cohort, at the end of autumn, may suppress the mortality associated with any KHV that is present and lead to a high prevalence of immunity in the population. Similarly, it may be possible to immunize uncontaminated cohorts cost-effectively and with minimal mortality by introducing KHV during this critical late autumn window.

We have considered the effectiveness of epidemic control strategies that halt disease progression in infected fish by artificially maintaining the water at a non-permissive temperature (33℃) for a fixed time when outbreak indicators exceed given thresholds. We have shown that, when the outbreak indicator is the number of dead fish, this control strategy is most effective if it is started as soon as the first dead fish is observed and maintained for a long time. The outbreak is well underway by the

time the first dead fish appear. A large part of the population is already in the infectious state, and the best strategy is to maintain this state for as long as possible to allow recovery, and prevent mortality. Using the number of infectious fish, including those that are in the ailing state, to determine when to start a single period of water temperature management can also result in effective outbreak control. In this case, the strategy is most effective if treatment is started when the number of infectious fish is close to the maximum of the uncontrolled outbreak, and maintained until the normal seasonal water temperature is decreasing into the non-permissive range for disease progression. As before, these conditions ensure that infection is widespread, but the majority of infected fish recover. If, however, treatment is started too soon or not maintained for the correct duration, mortality may exceed that of the uncontrolled epidemic if fish are held in the latent state until the temperature becomes permissive again for disease progression. This effect can be avoided if fixed periods of temperature control are applied every time the number of infected fish exceeds the critical threshold.

Our model is based on data from laboratory studies of koi herpesvirus. There are, however, areas of uncertainty. We assumed that only infectious and ailing fish can recover and gain immunity. We based this assumption on experiments conducted by St Hilaire et al. (2009) in which they briefly exposed fish to KHV at 21°C and then reduced the temperature to 12°C. They found that, 10 weeks after exposure, seroprevalence increased in a single jump from 0 to approximately 30%. After a further 15 weeks they increased the temperature to a permissive level for KHV progression. Subsequently there was approximately 40% mortality due to KHV. These observations suggest that temperatures that are not permissive for the general progression of KHV are permissive for the slow development of a measurable immune response following an initial challenge. However, it is not clear from these experiments whether the fish with antibodies had actually recovered from the infection, or possessed any immunity to re-infection. We modified our model such that fish in the latent state recover and gain immunity at the same rate as those in the infectious and ailing states. We found that mortality is still lowest, and immunity highest, in contaminated cohorts established in late autumn (Fig. S10); large, postponed, outbreaks still occur even if contaminated cohorts are established in winter (Fig. S10); single treatment control strategies are still most efficient when treatment duration is around 155 days (Fig. S11); the value of the

threshold $(I + A)^*$ at which the control efficiency is greatest is lower than when fish in the latent state cannot recover (Fig. S11) because the optimal strategy is to begin the treatment when (E+I) is close to its maximum. We have also assumed that the transmission process itself does not depend on temperature. We were unable to find experimental evidence for or against this assumption, and so took the most parsimonious approach. Exploring the possibility of temperature dependent transmission and its implications may be a worthwhile area of future experimental and theoretical research. Finally, we have not considered the economic implications of outbreak control by water temperature management. Maintaining elevated water temperatures is costly, particularly for long treatment periods. It may also decrease the yield from the cohort by interfering with the development of the fish. Conditions for optimal control of KHV to maximize profit could be explored by integrating these economic factors into the epidemiological model. In this paper, we do not assume specific environment as rivers, lakes and tanks, we can control water temperature by temporal transportation of fishes to tank where water temperature is controllable, this way might be effective in terms of economical cost.

In conclusion, disrupting normal seasonal patterns in water temperature can be an effective strategy for controlling koi herpesvirus. Seasonal patterns may also be exploited, possibly in combination with temperature management, to induce widespread immunity to KHV in a cohort of fish. However, employing these methods successfully requires careful assessment to ensure that the treatment is started, and finished, at the correct time. Errors in the timing can render the treatment ineffective, or counterproductive.

References

Adams, B. and Boots, M. 2007, The influence of immune cross-reaction on phase structure in resonant solutions of a multi-strain seasonal SIR model. *J. Theoret. Biol.* **248**, 202-211.

Altizer, S., Dobson, A., Hosseini, P., Hudson, P., Pascual, M. and Rohani, P., 2006, Seasonality and the dynamics of infectious diseases. *Ecol. Letters*. **9,** 467 – 484.

Aron J.L. and Schwartz I.B., 1984, Seasonality and period-doubling bifurcations in an epidemic model. *J. Theoret. Biol.* **110**, 665–679.

Dietz K., 1976, The incidence of infectious diseases under the influence of seasonal fluctuations., *Lecture Notes Biomathematics* **11**, 1-15. Berlin-Heidelberg-New York; Springer.

Gilad O, Yun S, Andree KB, Adkinson A, Zlotkin A, Bercovier H, Elder A, Hedrick RP., 2003, Molecular comparison of isolates of an emerging fish pathogen, koi herpesvirus, and the effect of water temperature on mortality of experimentally infected koi. *J. Gen. Virol*. **84**, 2661-2667

Greenman, J., Kamo, M. and Boots, M., 2004. External forcing of ecological and epidemiological systems: a resonance approach. *Physica D*. **190**, 136 – 151.

Haenen O. L. M., Way K., Bergmann S. M. and Ariel E., 2004, The emergence of koi herpesvirus and its significance to European aquaculture, *Bull. Eur. Ass. Fish Pathol.*, **24(6)**, 293-307.

Hedrick R. P., 2002. Initial characteristics of koi herpesvirus and development of a polymerase chain reaction assay to detect the virus in koi, *Cyprinus carpio koi*. *Dis. Aquat. Organisms*, **48**, 101-108.

Hethcote H. W. and Yorke J. A., 1980, Gonorrhea Transmission Dynamics and Control, Springer, New York

Iida, T., Sano, M., 2005. Koi herpesvirus disease. Uirusu **55**, 145–151.

Keeling M. J., Rohani P. and Grenfell B.T., 2001, Seasonally forced disease dynamics explored as switching between attractors. *Physica D* **148**, 317–335.

Kot, M. 2001, Elements of mathematical ecology. Cambridge University Press.

London W. P. and Yorke J. A., 1973, Recurrent outbreaks of measles, chickenpox and mumps. I. Seasonal variation in contact rates. *Amer. J. Epidemiol* **98**, 453-468

Miyakazi T., Okamoto H., Kageyama T. and Kobayashi T., 2000. Viremia-associated

Ana-Aqki-Byo, a new viral disease in color carp *Cyprinus carpio* in Japan. *Dis. Aquat. Organisms*, **39(3)**, 188-192.

Nisbet R. M. and Gurney W. S., 1983, The systematic formulation of population models for insects with dynamically varying instar duration. *Theor. Pop. Biol.* **23**, 114-135

Nisbet R. M. and Gurney W. S., 1982, Modelling Fluctuating Populations, Wiley, New York,

Oh M.J., Jung S.J., Choi T.J., Kim H.R., Rajendran K.V., Kim Y.J., Park M.A. and S.K. Chun, 2001, A viral disease occurring in cultured carp *Cyprinus carpio* in Korea. *Fish Pathol.*, **36(3)**, 147-151.

Peteri, A., 2005, Cultured Aquatic Species Information Programme. *FAO Fisheries and Aquaculture Department* [online]. Rome. Updated 12 July 2005. [accessed 22 July 2010]. http://www.fao.org/fishery/culturedspecies/Cyprinus_carpio/en

Pikarsky E., Ronen A., Abramowitz J., Levavi-Sivan B., Hutoran M., Shapira Y., Steinitz M., Perelberg A., Soffer D. and Kotler M., 2004, The pathogenesis of acute viral diseases in fish induced by the carp interstitial nephritis and gill necrosis virus, *J. Virol.* **78,** 9544–9551.

Ronen A., Perelberg A., Abramowitz J., Hutoran M., Tinman S., Bejerano I., Steinitz M. and Kotler M., 2003, Efficient vaccine against the virus causing a lethal disease in cultured *Cyprinus carpio*, *Vaccine* **21**, 4677–4684.

Schwartz I. B., 1985, Multiple stable recurrent outbreaks and predictability in seasonality forced nonlinear epidemics models. *J. Math. Biol.* **21,** 347–361.

St-Hilaire S., Beevers N., Joiner C., Hedrick R P., and Way K., 2009, Antibody response of two populations of common carp, *Cyprinus carpio* L., exposed to koi herpesvirus, *Journal of Fish Disease* **32**, 311-320.

Taylor N.G.H., Dixon P.F., Jeffery K.R., Peeler E.J., Denham K.L. and Way K., 2009, Koi herpesvirus: distribution and prospects for control in England and Wales. *J. Fish Diseases* **33**, 221-230.

Walster C., 1999. Clinical observations of severe mortalities in koi carp, *Cyprinus carpio*, with gill disease. *Fish Vet. J.*, **3**, 54-58.

Waltzek TB, Kelley GO, Stone DM, Way K, Hanson L, Fukuda H, Hirono I, Aoki T, Davison AJ, Hedrick RP., 2005, Koi herpesvirus represents a third cyprinid

herpesvirus (CyHV-3) in the family Herpesviridae. *J. Gen. Virol.*, **86**, 1659–1667.

Yuasa K., Ito T. and Sano M., 2008. Effect of water temperature on mortality and virus shedding in carp experimentally infected caps with koi herpes virus. *Fish Pathology*, **43 (2)**, 83-85

Supplementary infromation.

Derivation of Model

Our model is closely based on a model for a stage-structured insect population with temperature dependent growth introduced by Nisbet and Gurney (1983). Here we review their derivation in the context of our epidemiological model.

Differential equations in terms of recruitment, maturation, death and recovery

We assume that fish can be in one of six possible states: susceptible (*S*), latently infected (*E*), infectious (*I*), ailing (*A*), recovered (*R*) or, implicitly, dead (*D*). The processes by which transitions between these states occur are infection, incubation, recovery, natural mortality and disease induced mortality. The waiting times associated with infection, mortality and recovery are exponentially distributed. The waiting times associated with incubation, which connects state *E* to state *I*, and state *I* to state *A*, are such that a cohort of fish that enter a given state at the same time all leave that state after exactly the same period, the duration of which depends only on water temperature. In order to evaluate the incubation periods when temperature varies with time, q is defined to be the intensity of a notional viremia such that q increases at a temperature dependent rate $\gamma(T(t)) = \gamma(t)$ and $q=q_E = 0$ at the transition from state *S* to *E*, $q=q_I$ at the transition from *E* to *I*, $q=q_A$ at the transition from *I* to *A*. $\rho(q,t)$ is then defined to be the density of fish with viremia q at time t.

The system can be written very generally in terms of the rates of total influx, or 'recruitment' $Q_X(t)$ (X = *S, E, I, A, R*), out-flux due to infection and incubation, or 'maturation' $M_X(t)$ and out-flux due to death and recovery $Z_X(t)$. There are no births in the model, so the recruitment into the *S* state is $Q_S(t) = 0$. Maturation form the S state is equal to recruitment into the *E* state occurs solely by infection. Individuals in the *I* and *A* states are infectious. Infection results in immediate transition from the *S* state to the *E* state. Contact is assumed to be density dependent. Hence $M_S(t) = Q_E(t) = \beta S(t)(I(t) + A(t))$. Maturation out of state *E* is identical to recruitment into state *I* and occurs when viremia intensity $q=q_I$. So $M_E(t) = Q_I(t) = \gamma(t)\rho(q_I,t)$. Similarly, maturation out of state *I* is identical to recruitment into state *A* and occurs when viremia intensity $q=q_A$. So $M_I(t) = Q_A(t) = \gamma(t)\rho(q_A,t)$. Recruitment into the *R* class is the result of recovery, which occurs at constant rate h in the *I* and *A* states.

Hence $Q_R(t) = \eta(I(t) + A(t))$.

Finally, natural mortality occurs in all states at rate m. In state *A* there is additional disease induced mortality at rate x. Hence $Z_S(t) = \mu S(t)$, $Z_E(t) = \mu E(t)$, $Z_I(t) = (\mu + \eta)I(t)$, $Z_A(t) = (\mu + \eta + \xi)A(t)$ and $Z_R(t) = \mu R(t)$. Then we can write the complete system as:

$$\begin{aligned}
\frac{dS}{dt} &= -Q_E(t) - Z_S(t), \\
\frac{dE}{dt} &= Q_E(t) - M_E(t) - Z_E(t), \\
\frac{dI}{dt} &= M_E(t) - M_I(t) - Z_I(t), \\
\frac{dA}{dt} &= M_I(t) - Z_A(t), \\
\frac{dR}{dt} &= Q_R(t) - Z_R(t).
\end{aligned} \tag{S5}$$

Finding $M_E(t)$ and $M_I(t)$

The maturation rates $M_E(t)$ and $M_I(t)$ are expressed in terms of the introduced variable $\rho(q,t)$. $\rho(q,t)$ can be re-written in terms of the durations of the latent and infectious periods, $\tau_E(t)$ and $\tau_I(t)$ respectively, where

$$q_I - q_E = \int_{t-\tau_E(t)}^{t} \gamma(\hat{t})d\hat{t}, \tag{S6}$$

$$q_A - q_I = \int_{t-\tau_I(t)}^{t} \gamma(\hat{t})d\hat{t}. \tag{S7}$$

To do this, the McKendrick – von Forster partial differential equation for $\rho(q,t)$ (e.g. Kot, 2001) is used. If $J(q,t)$ is the flux, in the direction of increasing *q*, of individuals with viremia intensity *q* at time *t* then

$$\frac{\partial \rho}{\partial t} = -\frac{\partial J}{\partial q} - \mu\rho. \tag{S8}$$

For $q > q_E$, the rate of increase of viremia is $\gamma(t)$. So $J(q,t) = \rho(q,t)\gamma(t)$. Hence

$$\frac{\partial \rho(q,t)}{\partial t} = -\frac{\partial}{\partial q}[\gamma(t)\rho(q,t)] - \mu\rho(q,t). \tag{S9}$$

For the *E* state this partial differential equation has boundary condition $\rho(q_E,t)=\frac{Q_E(t)}{\gamma(t)}$ and can be solved (for details see Nisbet and Gurney, 1983) to give

$$\rho(q,t)=\frac{Q_E(t-\tau_E(q,t))}{\gamma(t-\tau_E(q,t))}\exp(-\int_{t-\tau_E(q,t)}^{t}\mu\,d\hat{t}) \tag{S10}$$

where $\tau_E(q,t)$ is the time already spent in the *E* state by a fish with viremia *q* at time *t*. By definition $\tau_E(t)=\tau_E(q_I,t)$. In addition, define $P_E(t)$ to be the proportion of the cohort that entered the *E* state at time $t-\tau_E(t)$ that actually matures at time *t*, rather than dying during the waiting period. So

$$\begin{aligned} P_E(t) &= \exp(-\int_{t-\tau_E(t)}^{t}\mu\,d\hat{t}), \\ &= \exp(-\mu\tau_E(t)). \end{aligned} \tag{S11}$$

Then, using (S11) and (S12)

$$M_E(t) = \gamma(t)\rho(q_I,t) = Q_E(t-\tau_E(t))\frac{\gamma(t)}{\gamma(t-\tau_E(t))}P_E(t). \tag{S12}$$

For the *I* state the McKendrick-von Foerster equations becomes

$$\frac{\partial\rho(q,t)}{\partial t}=-\frac{\partial}{\partial q}[\gamma(t)\rho(q,t)]-(\mu+\eta)\rho(q,t) \tag{S13}$$

with boundary condition $\rho(q_I,t)=\frac{Q_I(t)}{\gamma(t)}=\frac{M_E(t)}{\gamma(t)}$. The solution of this equation is

$$\rho(q,t)=\frac{M_E(t-\tau_I(q,t))}{\gamma(t-\tau_I(q,t))}\exp(-\int_{t-\tau_I(q,t)}^{t}\mu+\eta\,d\hat{t}) \tag{S14}$$

where $\tau_I(q,t)$ is the time already spent in the *I* state by a fish with viremia *q* at time *t*. By definition $\tau_I(t)=\tau_I(q_A,t)$. In addition, define $P_I(t)$ to be the proportion of the cohort that entered the *I* state at time $t-\tau_I(t)$ and actually matures at time *t*, rather than dying or recovering during the waiting period. So

$$P_I(t) = \exp(-\int_{t-\tau_I(t)}^{t} \mu + \eta \, d\theta), \\ = \exp(-(\mu+\eta)\tau_I(t)). \quad . \tag{S15}$$

Then

$$M_I(t) = \gamma(t)\rho(q_I,t) = M_E(t-\tau_I(t))\frac{\gamma(t)}{\gamma(t-\tau_I(t))}P_I(t) \\ = Q_E(t-\tau_E(t-\tau_I(t))-\tau_I(t))\frac{\gamma(t)}{\gamma(t-\tau_E(t-\tau_I(t))-\tau_I(t))}P_E(t-\tau_I(t))P_I(t). \tag{S16}$$

Using (S6), (S7), (S11), (S12), (S15) and (S16) system (S5) can be written as a set of integro-differential equations

$$\begin{aligned}
\frac{dS}{dt} &= -\beta S(t)[I(t)+A(t)] - \mu S(t), \\
\frac{dE}{dt} &= \beta S(t)[I(t)+A(t)] - \beta S(t_E^-)[I(t_E^-)+A(t_E^-)]\frac{\gamma(t)}{\gamma(t_E^-)}P_E(t) - \mu E(t), \\
\frac{dI}{dt} &= \beta S(t_E^-)[I(t_E^-)+A(t_E^-)]\frac{\gamma(t)}{\gamma(t_E^-)}P_E(t) \\
&\quad - \beta S(t_{EI}^-)[I(t_{EI}^-)+A(t_{EI}^-)]\frac{\gamma(t)}{\gamma(t_{EI}^-)}P_E(t_I^-)P_I(t) - (\mu+\eta)I(t), \\
\frac{dA}{dt} &= \beta S(t_{EI}^-)[I(t_{EI}^-)+A(t_{EI}^-)]\frac{\gamma(t)}{\gamma(t_{EI}^-)}P_E(t_I^-)P_I(t) - (\mu+\eta+\xi)A(t), \\
\frac{dR}{dt} &= \eta(I(t)+A(t)) - \mu R(t),
\end{aligned} \tag{S17}$$

where

$$t_E^- = t - \tau_E(t), \\ t_I^- = t - \tau_I(t), \\ t_{EI}^- = t - \tau_I(t-\tau_E(t)) - \tau_I(t).$$

Transforming the integrals to differential equations

The system (S17) can be transformed into a set of delay differential equations if differential equations are written for the integral terms $\tau_E(t), \tau_I(t), P_E(t)$ and $P_I(t)$. For $\tau_E(t)$, differentiating (S6)

$$0 = \gamma(t) - \gamma(t - \tau_E(t))\left(1 - \frac{d\tau_E(t)}{dt}\right). \quad \text{(S18)}$$

Rearranging

$$\frac{d\tau_E(t)}{dt} = 1 - \frac{\gamma(t)}{\gamma(t - \tau_E(t))}. \quad \text{(S19)}$$

Similarly

$$\frac{d\tau_I(t)}{dt} = 1 - \frac{\gamma(t)}{\gamma(t - \tau_I(t))}. \quad \text{(S20)}$$

Fitting to experimental data

Estimation of delay times

We estimated durations of the *E* and *I* states, τ_E^* and τ_I^*, at fixed temperatures from experimental results reported Yuasa et al. (2008), shown as $1/\tau_E^*$ and $1/\tau_I^*$ in Fig. 1a,b. We interpreted their observation that no KHV infection was detected at 13 °C and 30 °C to mean that no disease progression was occurring. We assumed that, for fixed temperature, viremia increases at a constant rate throughout the *E* and *I* states. We defined the notional viremia threshold for the transition from *E* to *I* to be $q_E = 1$. We then made the simplifying approximation that ratio of the latent and infectious delays is independent of temperature. So the notional viremia intensity required for the transition from *I* to *A* is given by $\frac{\tau_I(T)}{\tau_E(T)} = \frac{q_I}{q_E} = q_I$. Using the delays reported at 23 °C, we thus set $q_I = 4$. We then used least squares to fit parameters w_1, w_2 and w_3 of a Weilbull function for the temperature dependent rate of increase of viremia

$$\gamma(T) = w_3 \exp\left(-\left(\frac{T}{w_2}\right)^{w_1}\right) T^{w_1 - 1} w_1 w_2^{-w_1} \quad \text{(S21)}$$

to the combined data set of $1/\tau_E^*(T)$ and $q_I / \tau_I^*(T)$.

Estimation of mortality and recovery rates

We also estimated disease induced mortality and recovery rates from the experimental results reported by Yuasa et al. (2008), as shown in Fig. 15c. They observed the time

between exposure and death at a constant temperature of 23 °C. The first dead fish was observed five days after exposure. Mortality saturated at 70% of the population 21 days after exposure. For a cohort exposed at time $t_0 = 0$, the rates of change of the proportion of the cohort in the *R* and *D* states are given by

$$\frac{dR}{dt} = \begin{cases} 0 & if \quad t < \tau_E \\ \eta I & if \quad \tau_E \le t \le \tau_E + \tau_I \\ \eta A & if \quad t > \tau_E + \tau_I \end{cases} \qquad \text{(S22)}$$
$$\frac{dD}{dt} = \begin{cases} 0 & if \quad t < \tau_E + \tau_I \\ \xi A & if \quad t \ge \tau_E + \tau_I \end{cases}$$

Taking $E(0) = 1$ and $R(0) = D(0) = 0$, and assuming there is no natural mortality, solving (S22) until the cohort moves from the *I* to the *A* state

$$R(\tau_E + \tau_I) = 1 - \exp(-\eta \tau_I). \qquad \text{(S23)}$$

So, the total proportion of the cohort entering state *A* is $1 - R(\tau_E + \tau_I)$ and, for $t > \tau_E + \tau_I$

$$\begin{aligned} R(t) &= R(\tau_E + \tau_I) + (1 - R(\tau_E + \tau_I)) \frac{\eta}{\eta + \xi} (1 - \exp(-(\eta + \xi)(t - \tau_E - \tau_I))), \\ D(t) &= (1 - R(\tau_E + \tau_I)) \frac{\xi}{\eta + \xi} (1 - \exp(-(\eta + \xi)(t - \tau_E - \tau_I))). \end{aligned} \qquad \text{(S24)}$$

We used nonlinear regression to estimate ξ and η for these expressions, with τ_E^* (23) and τ_I^* (23) as above, from the time series of cumulative mortality reported by Yuasa et al (2008).

Figure Legends

Figure 15: Key epidemiological characteristics as functions of time. Gray curves and the right hand axes denote water temperature (T). (a) Forward delays in the exposed (dashed) and infectious (solid) states ($\hat{\tau}_E$ and $\hat{\tau}_I$ respectively); (b) Effective reproductive number $R_e(t)$; (c) Total proportion of the cohort that dies due to KHV (true line) and recovers (broken line) within two years, when the cohort is established at time t_0 and contains one infectious individual.

Figure 16: Progression of epidemic following the establishment of a cohort containing one infectious individual on day 250. Lines show the proportion of the population that is exposed (E, solid), infectious (I, dashes), ailing A (dot-dash) and recovered (R, dots).

Figure 17: Impact of treatment. Total mortality due to KHV over two years of aquaculture as a function of the epidemic threshold at which temperature control treatment is started (horizontal axis) and the duration of this treatment (vertical axis). Shading denotes mortality relative to the case without treatment. Black indicates reduced mortality, white indicates excess mortality. Cohorts were established at $t_0 = 90$ and included one infectious individual. (a) Threshold for starting treatment defined in terms of the instantaneous frequency of infectious fish, $(I + A)^*$. (b) Threshold defined in terms of the cumulative frequency of dead fish due to KHV, D^*.

Figure 18: Backward delays resulting from the combination of seasonality and treatment. The duration of the E and I states, τ_E (dashed) and τ_I (solid) respectively, as functions of time. A fish that moves from the E state to the I state at the time indicated on the horizontal axis was initially infected τ_E days before, where τ_E is the value indicated on the vertical axis. The interpretation of τ_I is similar. Treatment was started on day 115 and ended on day 275.

Figure 19: Impact of up to two treatment bouts. (a) Total mortality due to KHV over two years of aquaculture as a function of the epidemic threshold at which temperature control treatments are started (horizontal axis) and the duration of this treatment (vertical axis). Shading denotes mortality relative to the case without treatment: black indicates reduced mortality, white indicates excess mortality. (b) Number of treatment

bouts used: white – two, gray - one, black - none. Cohorts were established at t_0 = 90 and included one infectious individual.

Figure S7: Key epidemiological characteristics of koi herpesvirus. (a) Rate of progression from the exposed to the infectious class ($1/\tau_E$) as a function of water temperature (*T*); (b) Rate of progression from the infectious to the ailing class ($1/\tau_I$) as a function of water temperature (*T*); (c) Cumulative mortality as a function of time since first exposure to infection at 23°C. In all panels, points are experimental results from Yuasa et al. (2008), lines are the model functions fitted with parameter values shown in Table 1.

Figure S8: Seasonal distribution of mortality depending on the time at which a cohort containing one infectious individual is established. The shading indicates the relative frequency of mortality due to KHV ($D(t)/\mathrm{Max}(D(t))$, $D(t)=\xi A(t)$) at the time indicated on the horizontal axis in a cohort established at the time indicated on the vertical axis. Black denotes high mortality, white denotes no mortality

Figure S9: Impact of up to three treatment bouts. (a) Total mortality due to KHV over two years of aquaculture as a function of the epidemic threshold at which temperature control treatments are started (horizontal axis) and the duration of each bout of this treatment (vertical axis). Shading denotes mortality relative to the case without treatment: black indicates reduced mortality, white indicates excess mortality. (b) Number of treatment bouts used: white – three, light gray – two, dark gray - one, black - none. Cohorts were established at t_0 = 90 and included one infectious individual.

Figure S10: Total proportion of the cohort that dies due to KHV (true line) and recovers (broken line) within two years if fish in state *E* can recover at the same rate as those in states *I* and *A*. The cohort is established at time t_0 and contains one infectious individual.

Figure S11: Impact of a single treatment bout if fish in state *E* can recover at the same rate as those in states *I* and *A*. Total mortality due to KHV over two years of aquaculture as a function of the epidemic threshold at which temperature control treatment is started (horizontal axis) and the duration of this treatment (vertical axis). The threshold for starting treatment is defined in terms of the instantaneous frequency of infectious fish, $(I + A)^*$. Shading denotes mortality relative to the case without treatment. Black indicates reduced mortality, white indicates excess mortality. Cohorts were established at $t_0 = 90$, and included one infectious individual.

Table 3 : Functions and parameter values used throughout this article. All rates are expressed per day.

Figure.

Figure 15

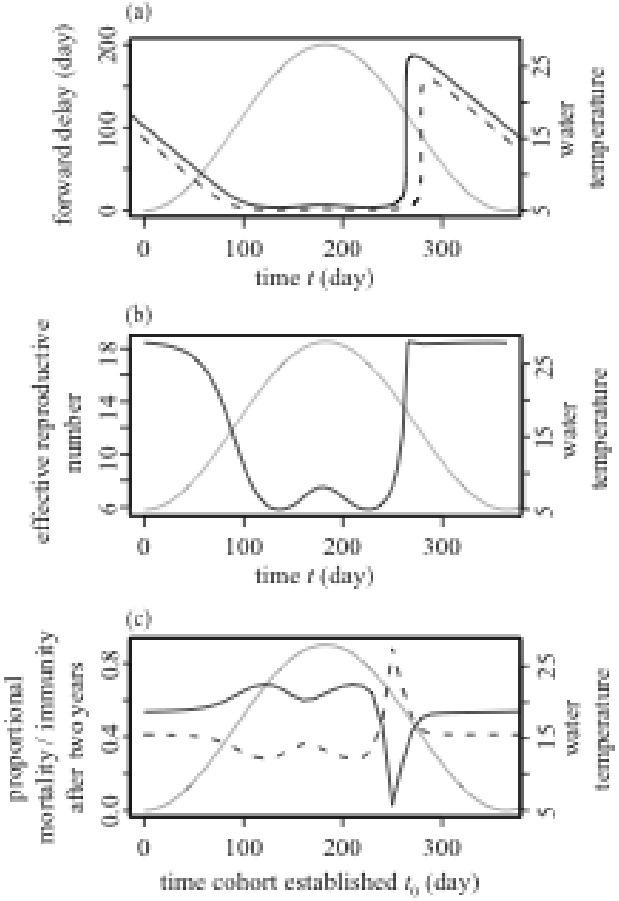

Figure 16

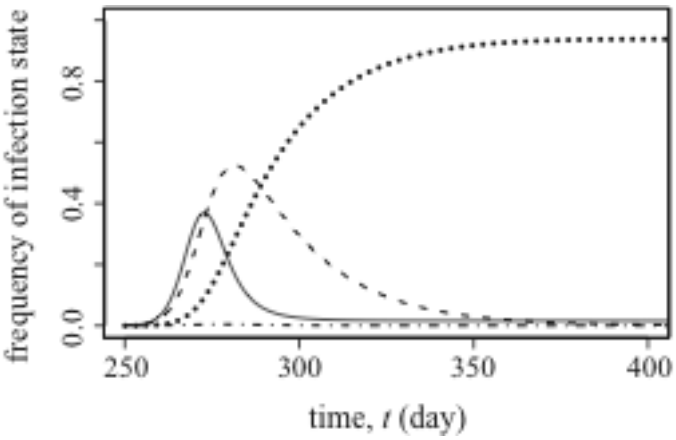

Figure 17

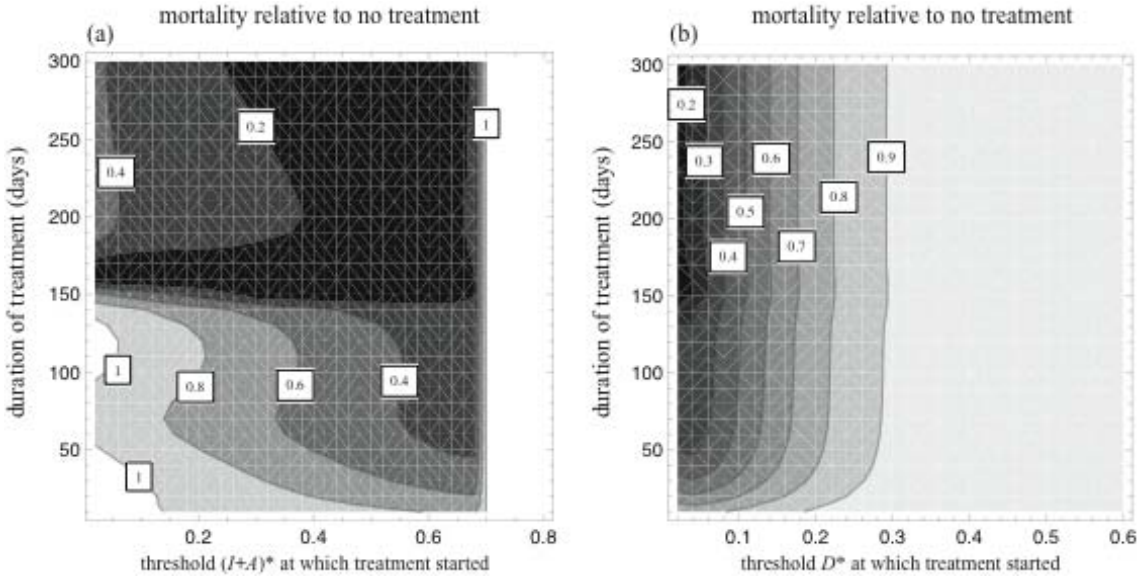

Figure 18

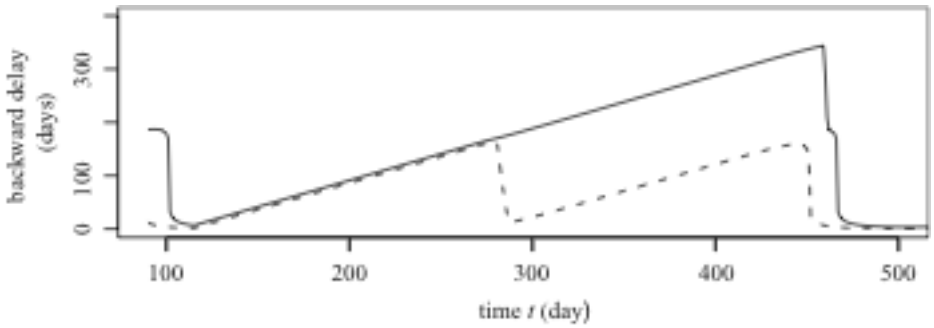

Figure 19

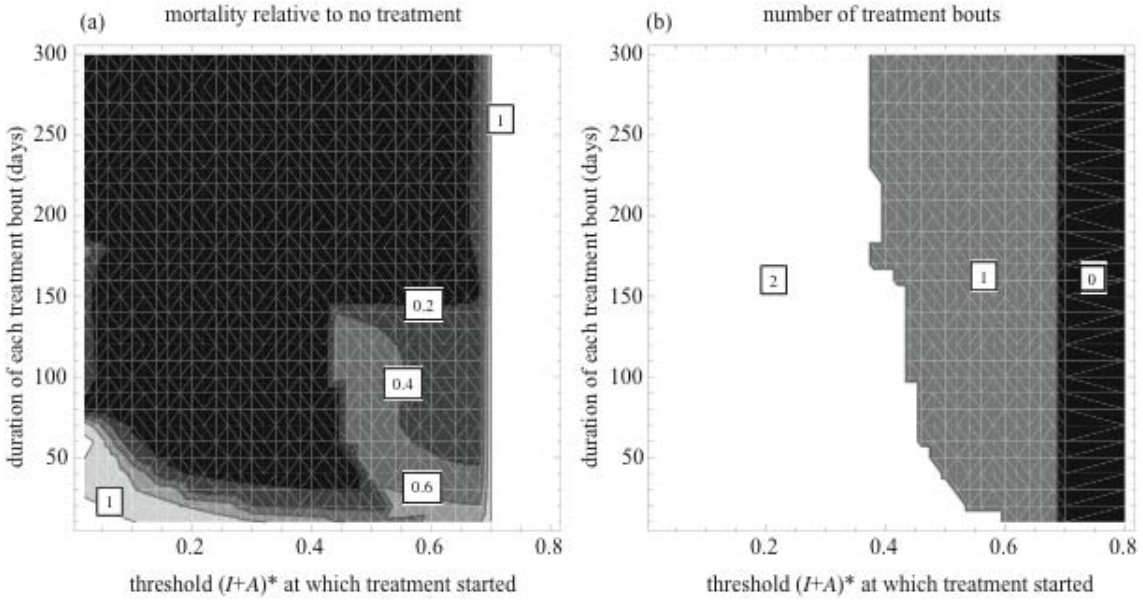
(a)
mortality relative to no treatment
300
250
200
150
100
50
duration of each treatment bout (days)
1
0.2
0.4
0.6
1
0.2
0.4
0.6
0.8
threshold (I+A)* at which treatment started
(b)
number of treatment bouts
300
250
200
150
100
50
duration of each treatment bout (days)
2
1
0
0.2
0.4
0.6
0.8
threshold (I+A)* at which treatment started

Figure S7

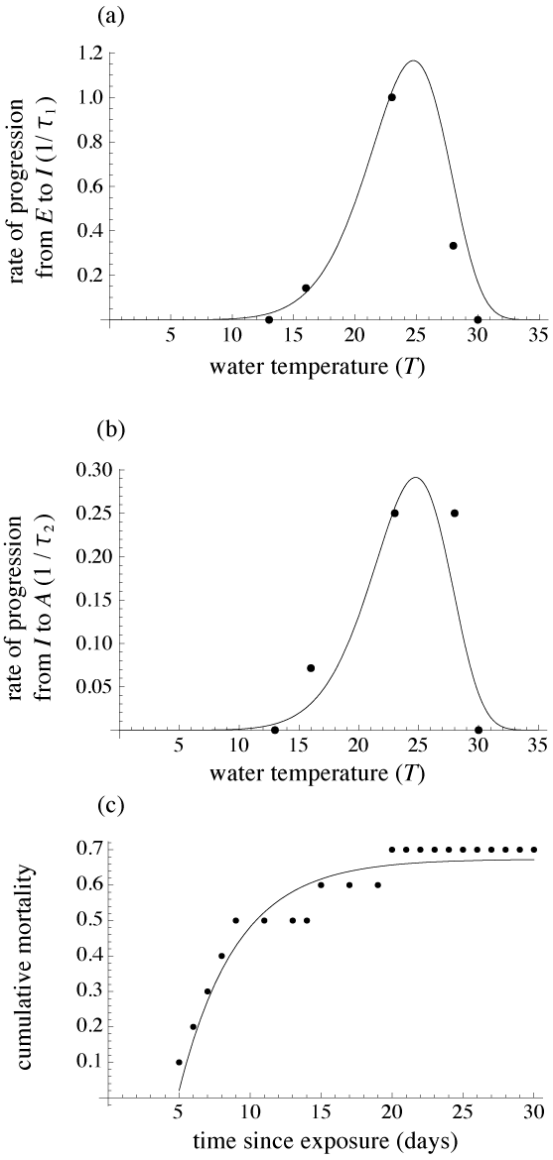
(a)
rate of progression from E to I ($1/\tau_1$)
water temperature (T)
(b)
rate of progression from I to A ($1/\tau_2$)
water temperature (T)
(c)
cumulative mortality
time since exposure (days)

Figure S8

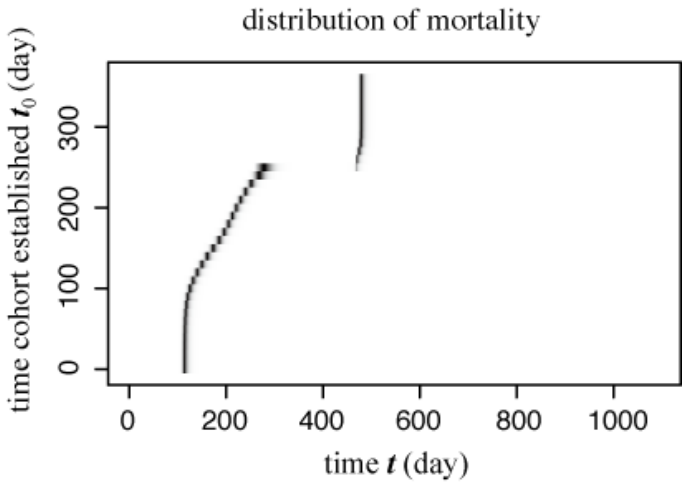

Figure S9

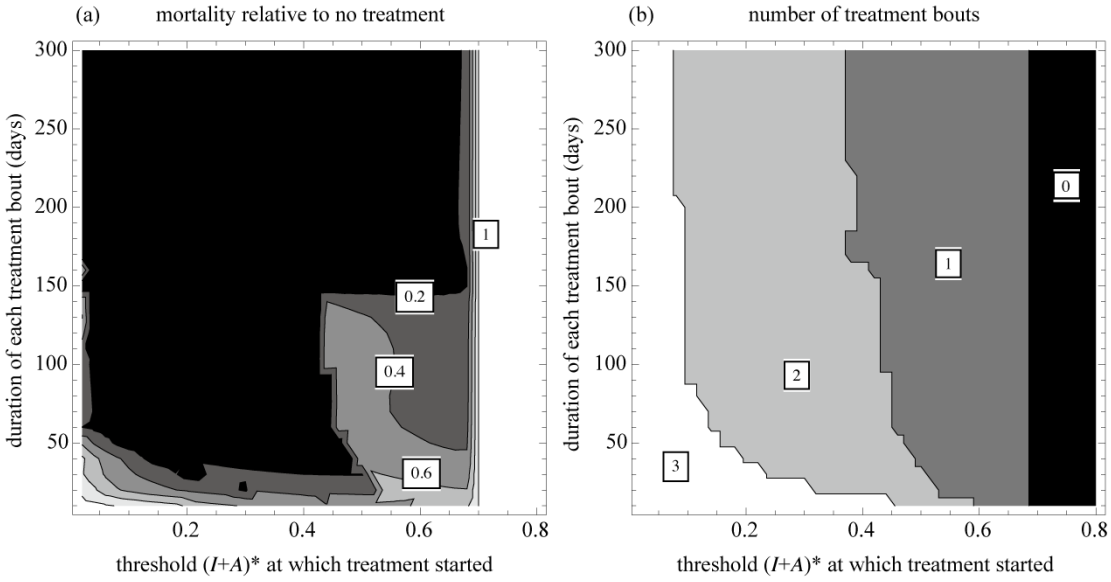

Figure S10

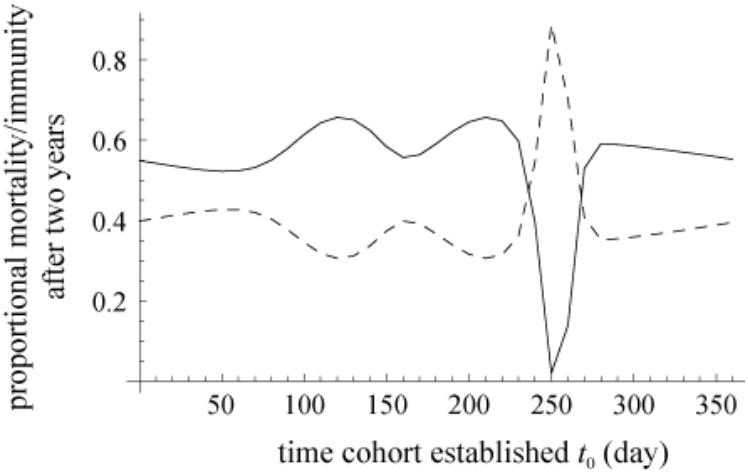

Figure S11

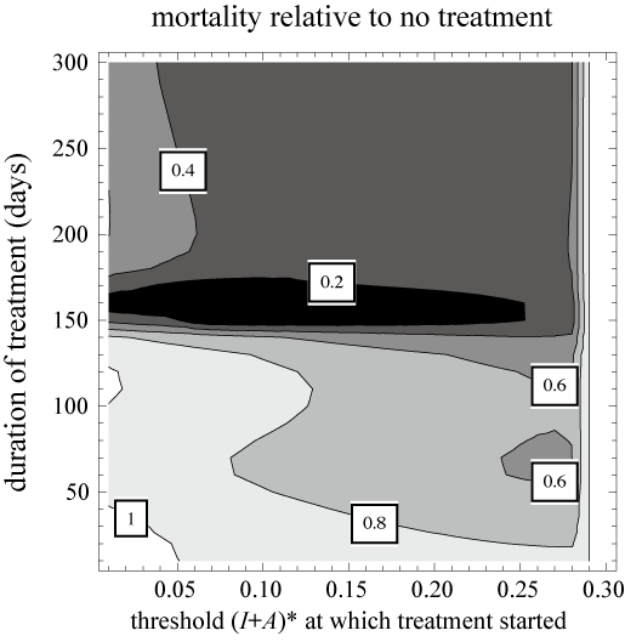

Table.

Table 3

Parameter	Meaning	Value
β	transmission rate	0.877
η	recovery rate	0.0467
ξ	morality rate due to KHV	0.2
μ	natural mortality rate	1/7300
$T(t)$	water temperature (°C)	$a-b\cos\left(\frac{2\pi t}{365}\right)$
a	a parameter of a	16.5
b	a parameter of b	11.5
$\gamma(T(t))$	rate of increase of viremia	$w_3\exp\left(-\left(\frac{T}{w_2}\right)^{w_1}\right)T^{w_1-1}w_1w_2^{-w_1}$
w_1	a parameter of γ	8.11
w_2	a parameter of γ	25.148
w_3	a parameter of γ	9.745

Acknowledgments

I would like to thank to Professors Akira Sasaki, Yoh Iwasa, and Mark Woolhouse for their very useful advise. I also thank to my collaborators, Dr Ben Adams and Dr Hiroshi Nishiura for their kind help for entire my works. I also thank to Brajendra Singh, Cheryl Gibbons, Isao Kawagushi, Jun Nakabayashi, Keisuke Ejima, Koichi Saeki, Koichiro Uriu, Mariano Siccolini, Masashi Kamo, Naoki Masuda, Sayaki Suzuki, Takahiro Irie, Takashi Uehara, Tsuyoshi Hirashima, Yoshihiro Morishita, members of mathematical biology laboratory in Kyushu University and members of SOKENDAI for their kind and useful comments. I also want to thank to my family, Etsuo Omori, Sachiko Omori and Yusuke Omori for warm encouragements.

Finally, I would like to thank the Precursory Research for Embryonic Science and Technology (PRESTO) Program of the Japan Science and Technology Agency (JST) and acknowledges a Grant-in-Aid for Scientific Research from the Japan Society for the Promotion of Science **(**JSPS) for financial support of this work.